Lawrence Berkeley Laboratory
UNIVERSITY OF CALIFORNIA

Accelerator & Fusion Research Division

Contributed to the Second Summer School on High-Energy Particle Accelerators, Stanford Linear Accelerator Center, Stanford, CA, August 2-13, 1982

THE TECHNOLOGY OF SUPERCONDUCTING ACCELERATOR DIPOLES

W.V. Hassenzahl, R.B. Meuser, and C. Taylor

June 1983

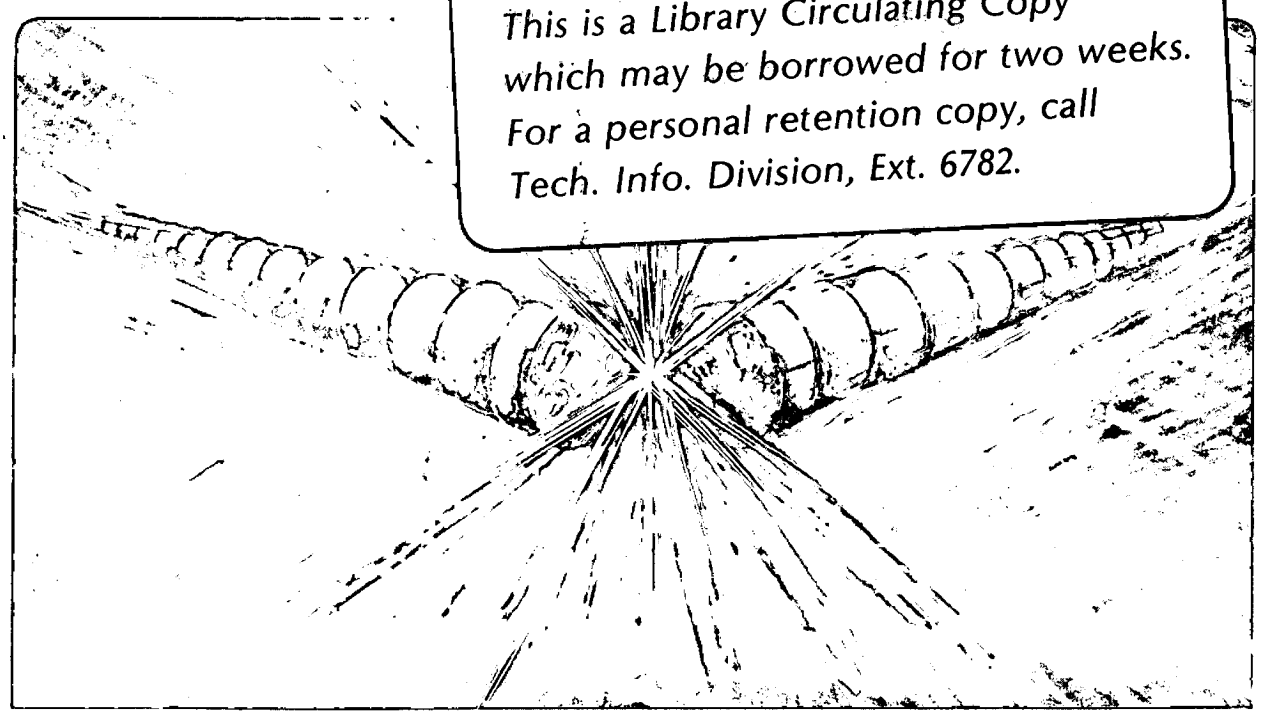

Prepared for the U.S. Department of Energy under Contract DE-AC03-76SF00098

DISCLAIMER

LBL-15987

THE TECHNOLOGY OF SUPERCONDUCTING ACCELERATOR DIPOLES*

W. V. Hassenzahl, R. B. Meuser and C. Taylor

June 1983

Accelerator and Fusion Research Division
Lawrence Berkeley Laboratory
University of California
Berkeley, California 94720

*This work was supported by the Director, Office of Energy Research, Office of High Energy and Nuclear Physics, High Energy Physics Division, U. S. Dept. of Energy, under Contract No. DE-AC03-76SF00098.

TABLE OF CONTENTS

APPENDIX

THE TECHNOLOGY OF SUPERCONDUCTING ACCELERATOR DIPOLES*

W. V. Hassenzahl, R. B. Meuser, and C. Taylor

I. INTRODUCTION

Superconducting magnets have been extensively used by high energy physics experimenters since the discovery in 1960 of several alloys and compounds capable of carrying practical current densities at high magnetic field. The initial rush to utilize these remarkable materials and current densities was frustrated by the degradation that was widely observed in the wire when it was wound into superconducting coils. The conductor in large coils often carried less current than when tested in short samples. This "unstable" behavior is now known to be caused by heat generated in superconducting wire when the magnetic field and current are changed. The amount of energy released is very small, but, because the superconductor is at a very low temperature, the specific heats of the magnet components are very small and local temperature excursions can cause a loss of superconductivity. The current passing through the resistive coil then causes Joule heating and leads to a rapidly spreading temperature increase or "quench". A small, local, transient temperature rise can ultimately result in the transition of an entire magnet winding from the superconductive to the resistive state.

*This work was supported by the Director, Office of Energy Research, Office of High Energy and Nuclear Physics, High Energy Physics Division, U. S. Dept. of Energy, under Contract No. DE-AC03-76SF00098.

To develop a technology of superconducting accelerator dipoles[1] and to understand their behavior during a transition we must study: 1. The basic properties of practical superconductors,[2] 2. their stability[3] and 3. the physical characteristics[4] of other magnet components. In this chapter some of the phenomena that lead to heat generation in magnets are explained, the material characteristics that affect coil performance are described, and several possible designs for accelerator dipoles are discussed.

In this chapter we discuss accelerator dipoles and their characteristics Other types of magnets, in particular bubble chamber magnets have been quite successful. Their performance is based on "cryogenic stability" which is addressed only briefly in this chapter. This type of stability is not available to the accelerator designer because of the large quantities of copper or other stabilizer that would reduce the current density in the windings to an unacceptably low value.

II. STABILITY

Superconducting magnets, which can function only at very low temperatures, are subject to thermal and mechanical disturbances that may cause all or part of the superconductor in the magnet to undergo a superconducting to normal transition or quench. Two major goals of superconductor and magnet design are: 1, to eliminate or at least reduce the frequency and magnitude of these disturbances, and 2, to reduce the susceptibility of the magnet system to these disturbances. The stability of a superconducting coil may thus be defined as the ability of the coil to withstand or recover from the effects of a disturbance.

The disturbances may be local or distributed and may be continuous or pulsed. The types of disturbances and the appropriate dimensions are given in Table 1. Obvious sources of disturbances includes resistive regions in the superconductor, conductor motion, eddy currents induced by field changes and flux motion and, for accelerator magnets, beam dumps.

If a disturbance causes some heating in the coil but does not drive the coil normal, the energy deposited must still be removed from the magnet to avoid any longtime temperature rise. The heat that is deposited in the magnet but does not quench it is referred to as a loss. This heat must be removed during cyclic operation.

TABLE I

The Units of Different Types of Disturbances Possible in a Superconducting Magnet

Temporal Characteristic	Spatial Characteristic	
	Point	Distributed
Transient	Joules	Joules/m^3
Continuous	Watts	Watts/m^3

The stability of a magnet and the losses in the magnet are closely related because there is simply a quantitive difference between the energy or power input leading to the two different results.

The ability of a coil to withstand a given heat input depends on many of the physical characteristics of the coil materials, in

particular superconductivity, specific heat or enthalpy, normal conductivity or resistivity, thermal conductivity, strength, elastic modulus, and the friction coefficients and heat transfer from one material to another. Though the precise quantitive values of each of these parameters is needed for a detailed magnet design, only the general trends and characteristics are important to understand the effects of these parameters on stability. Therefore, some of these characteristics are described briefly in a subsection at the end of this chapter.

The stability of a superconductor depends on the maintenance of the combination of current, field, and temperature below a combined limit. This is best seen in Fig. 1. The surface shown represents the boundary between the superconducting and normal state. The goal of the magnet designer is to keep the superconductor in the superconducting state or to have it return to this state if there is a disturbance that raises the temperature to too high a value. In general current and field transients can drive a coil normal just as increased temperature does. However, large changes in these parameters are needed so they only affect performance near the field or current limit. The stability of a magnet thus depends on maintaining the temperature low enough to assure the superconducting state. Several disturbances, as mentioned above, can cause the superconductor to heat up and become normal. Each of these will be discussed below.

First let us look at a tiny filament of superconductor embedded in a normal conducting matrix and make an approximation that it is a slab instead of a circular filament. In our model of superconductivity, the local current that flows in the conductor can be either zero or the

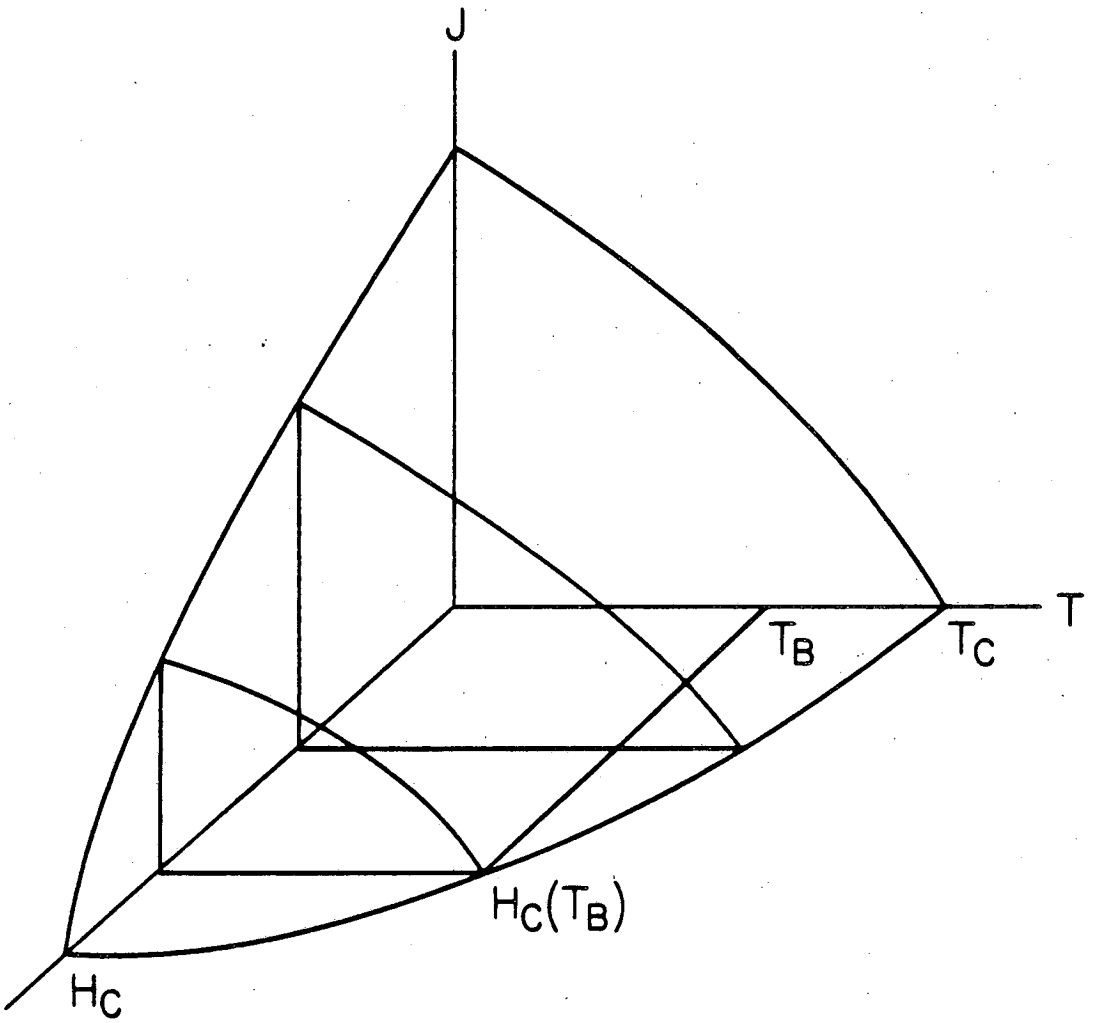

XBL 836-10137

Fig. 1. Critical current density in a superconductor as a function of temperature and magnetic field - T_C is the critical temperature at zero field and zero current, and H_C is the critical field at zero temperature and zero current. When operating at a bath temperature T_B, the critical field is reduced to $H_C(T_B)$.

critical current. This local current can be a shielding current to keep magnetic flux from entering the conductor or can be a net current flowing in the conductor. When a small current flows in the conductor it is all at the surface and penetrates deeper as the current increases; this is shown in Fig. 2a. A more complicated situation is shown in Fig. 2b where the field, which is a maximum at the surface, is seen to decrease with depth in the conductor; and the shielding currents on different sides of the conductor are in opposite directions. As the current, or the field, or both are increased there is a motion of flux across the surface current that results in some energy dissipation and heats the conductor. The subsequent temperature rise decreases the critical current and thus allows flux to penetrate further into the superconductor. The events described above are shown in a general case in Fig. 3.

The criteria for stability is that the amount of heat released by a given flux motion will cause a smaller amount of flux to enter the conductor than entered in the original disturbance. If more flux is allowed to penetrate then an "avalanche" occurs and the conductor is quickly heated to the normal state.

To determine in a quantitive sense the parameters that affect stability against this type of disturbance we consider a slab having a thickness 2a, and an external field B on each side as shown in Fig. 4. A small temperature rise will allow additional flux to penetrate the superconductor because the critical current decreases.

A stability criteria can be derived, based on the condition that the energy deposited when the maximum flux enters the superconductor is less than the enthalpy of the superconductor between the operating

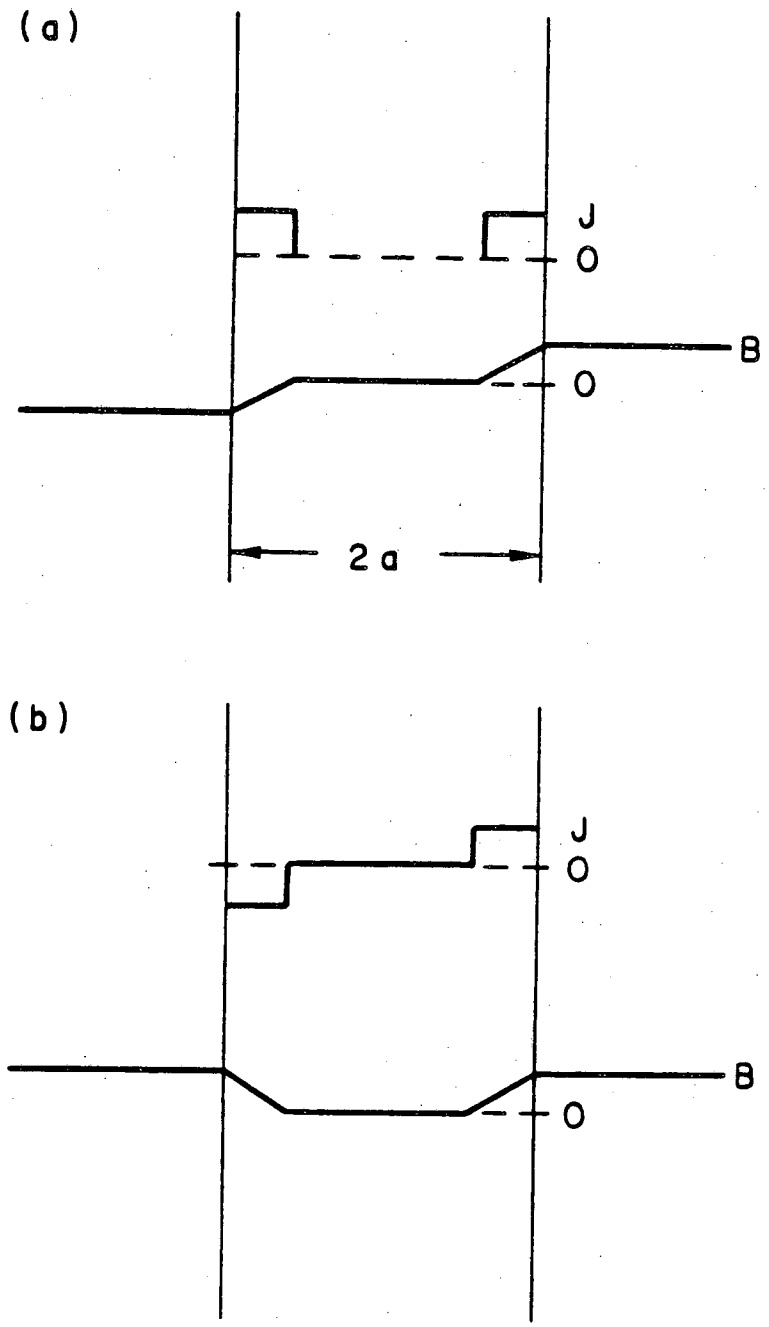

XBL 836-10135

Fig. 2a. Field and current in a current-carrying superconducting slab.

Fig. 2b. A superconductor in a magnetic field generates a shielding current at its surface that excludes flux from its center.

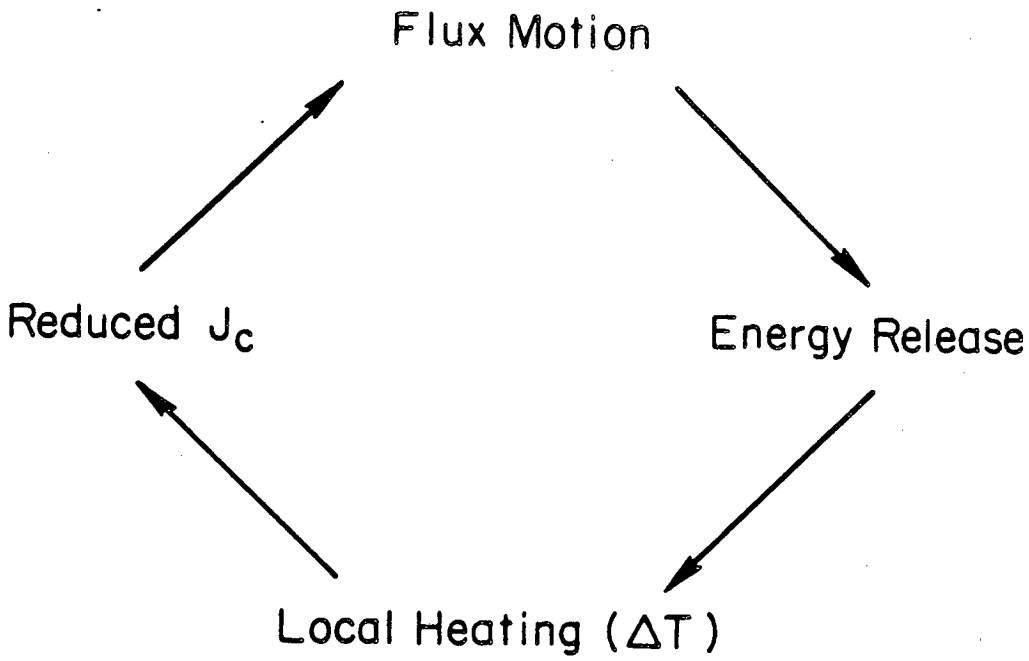

XBL 836-10134

Fig. 3. The sequence of events in a "Flux Jump". The criterion for stability is that the secondary flux motion generated by a disturbance be less than the initial motion.

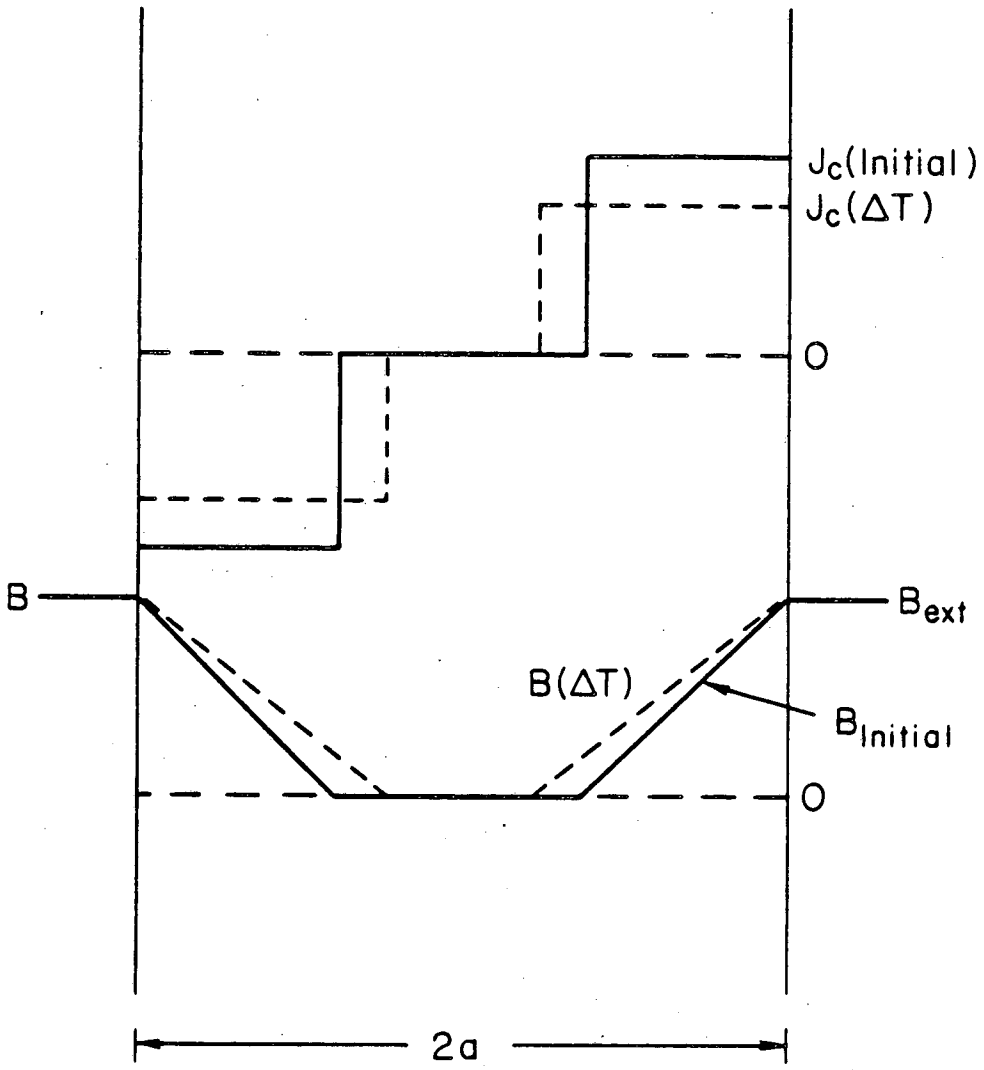

XBL 836-10136

Fig. 4. The effect of flux motion or a temperature rise on the current and flux distribution within a superconductor.

temperature and the critical temperature. The stability relation is:

$$\frac{\mu_o j_c^2 a^2}{\rho C_p (T_c - T_o)} \leqslant 3$$

where j_c is the critical current density (A/m^2), $2a$ is the slab thickness (m), the product ρC_p is the specific heat per unit volume (J/m^3) and T_c is the critical temperature. The question is, "how large can the filament be under the operating condition in the magnet?" We give examples here of the maximum stable filament size for Nb-Ti at 4.2 and 1.8K as shown in Table II, using data taken from the section below on material characteristics.

TABLE II

The Maximum Stable Nb-Ti Filament Size (μm) at 4.2 and 1.8K

Temperature (K)	4.2	1.8	1.8
Field (T)	6	6	8
Critical Temperature (K)	6.5	6.5	4
j_c (A/m^3)	1.5×10^9	2.5×10^9	1.5×10^9
ρC_p (J/m^3)	5.4×10^3	6×10^2	6×10^2
Radius (μm)	115	47	38

Generally, in designing a conductor one attempts to use a filament size that is less than the value given here, say half or less. The reason is that this type of instability, which is called a flux jump, seems to occur at low and intermediate fields where the critical current is

very high. (In fact, as will be seen below, keeping the ac losses in the conductor below an acceptable level is often more restrictive than the flux jump limit.)

Because the size of the filaments that affects the stability of the conductor depends on the specific heat or enthalpy of the superconductor itself, the use of fine filaments is called enthalpy stabilization. Using the formula above, the relationship between temperature and field can be predicted as shown in Fig. 5. Experimentally observed flux jump fields are shown to agree quite well with this theory.

Early superconducting wires usually had one filament and the larger wires were generally unstable. The theory of enthalpy stabilization, which was first developed by Wilson in the late 60's, led to the use of superconducting wires with many fine filaments, as shown in Fig. 6.

The superconductor is usually imbedded in a normal conducting matrix that serves several purposes. Mainly it is there to carry current when one or more of the filaments goes normal. The calculation above for the stability of each filament also applies to the composite strand because the many filaments in the strand are coupled electrically by the normal conductor.

By twisting the strand the flux jumps due to external field can be limited to a conductor section shorter than the twist length, which is usually a few conductor diameters. (The twisted conductor has a smaller flux linkage between strands resulting in smaller eddy currents and reduced ac losses.) There is, however, a problem associated with penetration of the flux generated by the conductor itself. The maximum strand self field must be limited to the flux jump field for a strand of radius r, or, following the previous calculation for a slab of

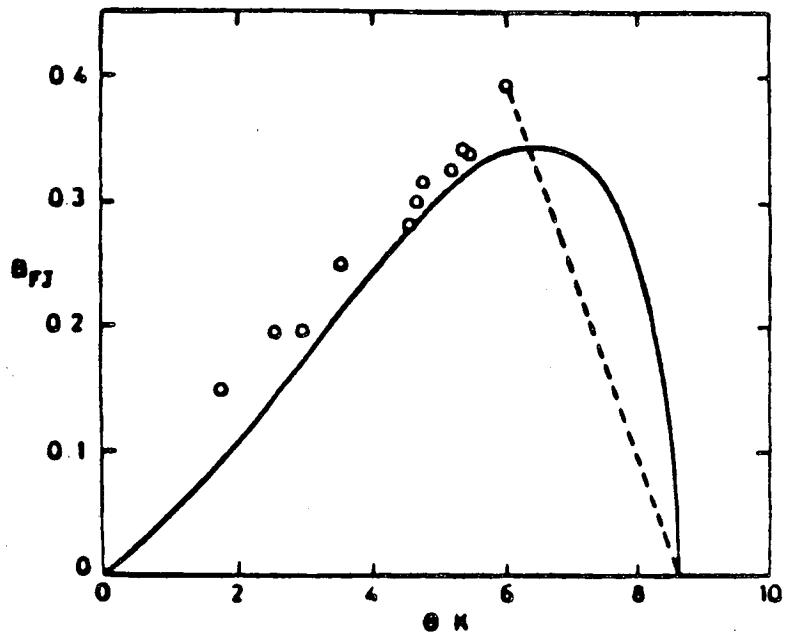

Fig. 5. Experimental measurements of the flux jumping field in NbTi compared with the theoretical value.

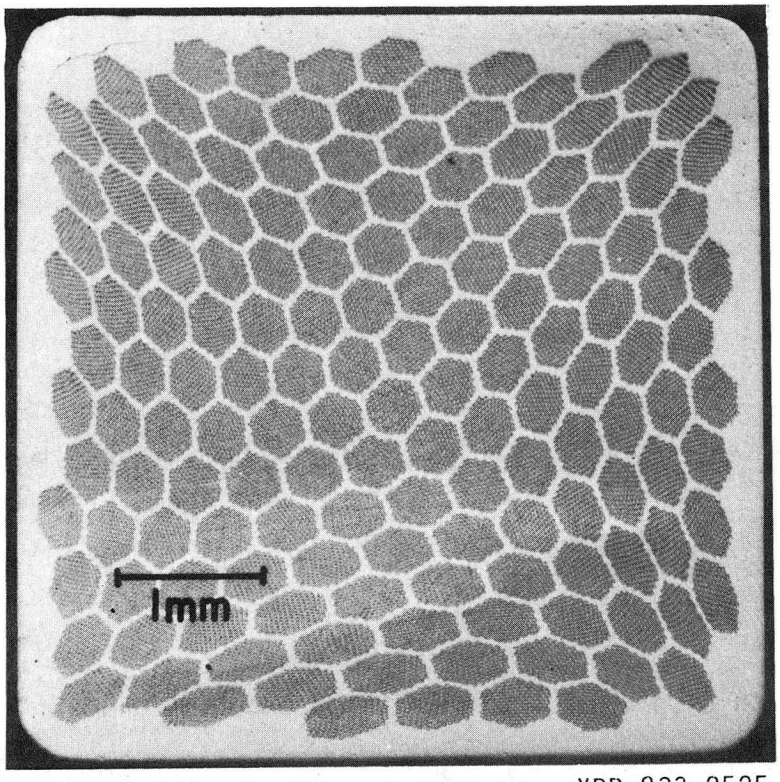

XBB 833-2525

Fig. 6. Cross section of a multifilamentary superconductor.

superconductor but including the specific heat and other stabilizer characteristics;

$$\frac{\mu_o \lambda^2 j^2 r^2}{\rho C_p (T_c - T_o)} \leq 12$$

where λ is the fraction of superconductor in the composite (normally, $\lambda \simeq 0.3$ to 0.5). Again, solving for a typical conductor:

$$2r \cong 0.5\text{mm}$$

If we solve the same problem for a circular conductor, the result is;

$$2r \simeq 2\text{mm}$$

In fact this solution is known to be wrong because it assumes there is no stabilizing affect from conductivity of the normal conductor and the flux motion is very fast. In practice this self-field limit is too small by about a factor of 2.

In addition to flux jumps, mechanical disturbances can also introduce heat into the conductor. The heat generated may be due to the conductors' motion in the field, or the frictional force between the conductor and its support. If enough heat is deposited a section may go normal. The stability of the coil then depends on the balance between cooling and heating within and near the normal region. The heating per unit volume after the disturbance is simply Joule heating of the form

$j^2\rho$, and the cooling is due to heat transfer to helium at the surface of the conductor and thermal conductivity along the conductor.

If the heating is greater than the cooling then the normal region will expand, and if the cooling is greater then the region will contract. We consider here only axial heat conduction (which applies to an epoxy impregnated coil) and devise an expression for the length of a normal region that can recover where k is the thermal conductivity and A is the cross section of the conductor, giving

$$j^2\rho AL \geq 2kA(T_c-T_o)/L$$

$$L^2 > \frac{2k(T_c-T_o)}{j^2\rho}$$

or $L \simeq 2mm$ for a 1 to 1, Nb-Ti to Cu composite.

Thus normal regions on the order of a few centimeters will expand. To give an example of the minute energy needed to drive a superconductor normal, using the data on specific heat, the energy required to raise the temperature of a 2mm length of Fermilab doubler conductor by 1K is about 10^{-5} J.

The source of heating as mentioned above can be wire motion. For the section of doubler conductor 2mm long, and at the operating current near 4000A and operating field of 5T, the energy released in motion is

$$I \times B\ \Delta s = 4000A\ 5T\ \Delta s$$

Assuming B, I, and the motion of the wire are all perpendicular, then the motion Δs required to release 10^{-5}J is about 2.5 μm.

Cracking of insulation such as epoxy, in particular the insulation in direct contact with the conductor, can deposit large amounts of heat in the conductor. The strain energy in the resin is on the order of, $\sigma^2/2E$, where σ is the stress and E is the Young's modulus. At 4K the modulus of epoxy is about 7×10^3 MPa (10^6 psi) and the yield stress of the epoxy bond is about 30 MPa (5000 psi). The elastic or strain energy is thus:

$$E_\sigma \approx 6\times10^{-5}\ \text{J/mm}^3$$

Thus, enough energy is available to initiate a normal zone in a Doubler cable if the stress in 0.16 mm^3 of epoxy is reduced to zero, by cracking for example.

There have been many calculations as above of the disturbance that might exist or of the size of disturbance that a conductor can withstand but few observations of real disturbances. The voltage observed across an accelerator dipole constructed at LBL is shown in Fig. 7. The energy associated with the pulse is $\int VI\ dt \approx 10J$. If we ascribe this to conductor motion it corresponds to several cubic centimeters moving.

Yet we observe only a small fraction of one turn going normal at first. Obviously all the energy associated with conductor motion does not go into the conductor, some of it goes into the power supply and into a readjustment of the magnetic field. The observed voltage spike is just a measure of the energy available in a disturbance.

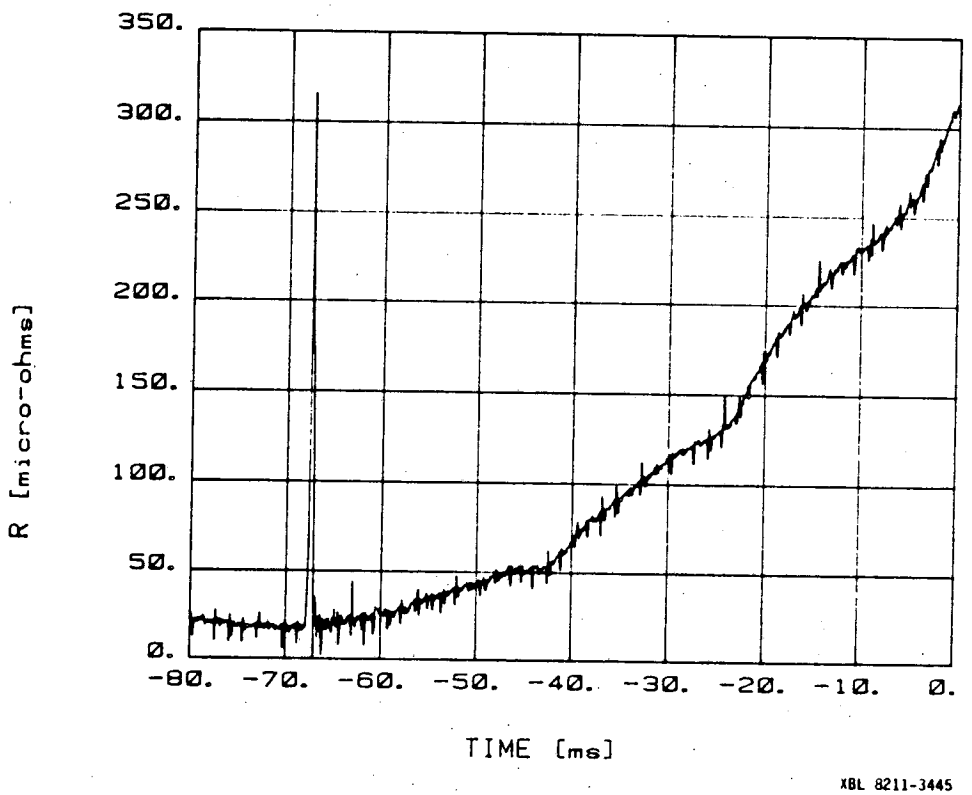

Fig. 7. Signal observed across a normal going region of the "north pole" of D-8A during a quench.

One last type of stability "cryostatic stability" is important in many large magnets such as bubble chamber and fusion magnets where relatively low current densities are possible. As the size of the magnet increases the regions that must be capable of recovering from a quench also increase. For a conductor to recover from a normal region without a magnet quench requires the local cooling to exceed the local heating. The heating is given by:

$$Q = I^2 R;$$

and the cooling is due to heat transfer to the helium bath

$$Q = A_h q ,$$

where A_h is the wetted surface area per unit length and q is the minimum heat flux that can be transmitted from the conductor to the helium. Using a fully exposed round wire as an example ($A = \pi r^2$, $A_h = 2\pi r$), and assuming the heat transfer is not dependent on surface orientation:

$$(j\ A)^2 \cdot \left(\rho \frac{L}{A}\right) \leq A_h\ q$$

or

$$r < \frac{2q_c}{j^2 \rho}$$

In practice the value of q_c depends on surface conditions and orientation and generally must be measured. The value of the

resistivity ρ is a characteristic of the stabilizing material and the magnetic field. Examples are given for both of these parameters below. The general dependence in the equation above however, gives some insight into the choice of operating current and conductor shape. The larger the conductor the smaller the stable current density or the current density at which it can recover.

III. LOSSES

The losses in superconducting coils can, in a general sense, be ascribed to current flowing through a resistive component. The most obvious resistance in a magnet is at joints or splices between two conductors. These joints may be necessary for two reasons: first they may facilitate coil fabrication, and second there may be restrictions on available conductor lengths. In most magnets the number of joints is small and the resistance of each joint is on the order of nano-ohms. In a Fermilab conductor, for example, the resistance of a 10cm-long joint, based on an effective solder thickness of 0.1 mm, will be about $10^{-8}\ \Omega$. At 5000A the power dissipated in the joint will be about 0.25W.

The resistance of superconducting materials is zero only when a continuous current is flowing. When currents change there is a flux flow in the filaments of superconductor that leads to a power dissipation.

The force required to "push" flux across the current flowing in the filament, JxB, integrated over the conductor can be expressed as a loss:

$$q = \frac{\text{loss}}{\text{vol}} = \frac{1}{a}\int_0^p J_c\, \Delta\phi\, dx = \mu_o \frac{p^3}{3a} ,$$

where p is the dimension of maximum flux penetration, $2a$ is the slab thickness, and J_c, B_p, and B_a are given by $J_c = B_p/2\mu_o p = B_a/2\mu_o a$. The change in flux $\Delta\phi$ a distance x out from the point of maximum penetration (refer to Fig. 4) is:

$$\Delta\phi = \mu_o J_c x^2$$

The loss during a full cycle is $2q$ or

$$Q = 2q = \frac{2}{3a}\mu_o{}^2 J_c{}^2 p^3 = \frac{B_p{}^2}{2\mu_o}\frac{p}{3a}$$

The ratio p/a is equal to the ratio of the maximum field in a cycle B_p to the field at complete penetration B_a. If we call this ratio β, then the loss per cycle is

$$Q = \frac{B_p{}^2}{2\mu_o}\frac{\beta}{3} .$$

This loss, which is called the hysteresis loss, has no time dependence and will be the same for a short as for a long cycle.

For a cycle that has a maximum field that exceeds the field at full penetration, $B_p > B_a$ the flux penetration is slightly different and the loss has a different characteristic. The flux is of the form $\Delta\phi = (B_p - B_a)x$, then, solving for the total loss we get

$$Q = 2\left(B_p - B_a\right) J_C \frac{a}{2} = \frac{B_p^2}{2\mu_o}\left(1 - \frac{1}{\beta^2}\right)\frac{1}{\beta} .$$

The total loss is the sum of these two, giving for a complete cycle

$$Q = \frac{B_p^2}{2\mu_o}\left\{\left(1 - \frac{1}{\beta^2}\right)\frac{1}{\beta} + \frac{\beta}{3}\right\}$$

$$= \frac{B_p^2}{2\mu_o}\left\{\frac{1}{\beta} - \frac{1}{\beta^3} + \frac{\beta}{3}\right\} = \frac{B_p^2}{2\mu_o}\,\Gamma(\beta) .$$

This function $\Gamma(\beta)$ is seen to have a peak at approximately full penetration, $\beta = 1$.

Just as the losses described above depend only on the superconductor, there are other losses associated with the current that flows in the normal, stabilizing conductor. These are due to eddy currents and can be calculated once the geometry and the resistivity of all the components are known. In addition to these single component loss mechanisms, there are currents induced that flow partly in the superconductor and partly in the normal matrix. Several different types of losses are described in the references.

The two major losses to be considered are:

- Self-field losses; which is due to the penetration into the conductor of the field it produces. The derivation is much the same as for the hysteresis loss described above.

- Coupling loss; which is due to the penetration into the conductor of an externally produced field.

This loss may be thought of as being due to current flowing over a relatively large distance in the superconductor and a short distance in the normal stabilizer.

In most conductors the major part of this loss is controlled by twisting the superconducting strands to limit the flux linking or coupling any circuit.

IV. QUENCHES AND QUENCH PROTECTION

The quench process in a large magnet is generally either a two or three dimensional propagation of a normal region through the coil windings, starting from either a local or a distributed disturbance. An expression for the propagation velocity of the quench was initially derived by Cherry and Gittleman for a thermal wavefront in a conductor under adiabatic conditions (i.e. a conductor embedded in epoxy).

$$V_{quench} = \frac{I(T_m - 2T_c)}{C} \sqrt{\frac{k \cdot \rho}{T_c \cdot T_m(T_m - T_c)}}$$

$$= \frac{I(T_m - 2T_c)}{C} \sqrt{\frac{L}{T_c(T_m - T_c)}}$$

where I is the current, k is the thermal conductivity, ρ is the resistivity, C is the specific heat, T_m is the difference between the maximum temperature in the quench region and the bath temperature, and T_c is the difference between the critical temperature and the bath temperature. The Lorenz relationship, which is described later in the section on thermal conductivity, has been used to simplify the expression.

The quench propagation velocity is reduced considerably in the presence of helium and also depends somewhat on conductor geometry and orientation. Figure 8 shows the observed dependence of quench velocity on operating current in a model accelerator dipole. The equation indicates the velocity should become infinite as the critical current or critical temperature is approached. In fact this doesn't occur because of several reasons, the most important of which is the normal variation of field within the coil so that conductor is in the peak field region over only a very short distance. The maximum quench velocity observed in conductors is about 60 m/s.

The quench also propagates from turn to turn and from layer to layer. The velocity of propagation perpendicular to the conductor depends on the relative thermal conductivities. Usually, there is some insulation between turns, and some helium and insulation between layers.

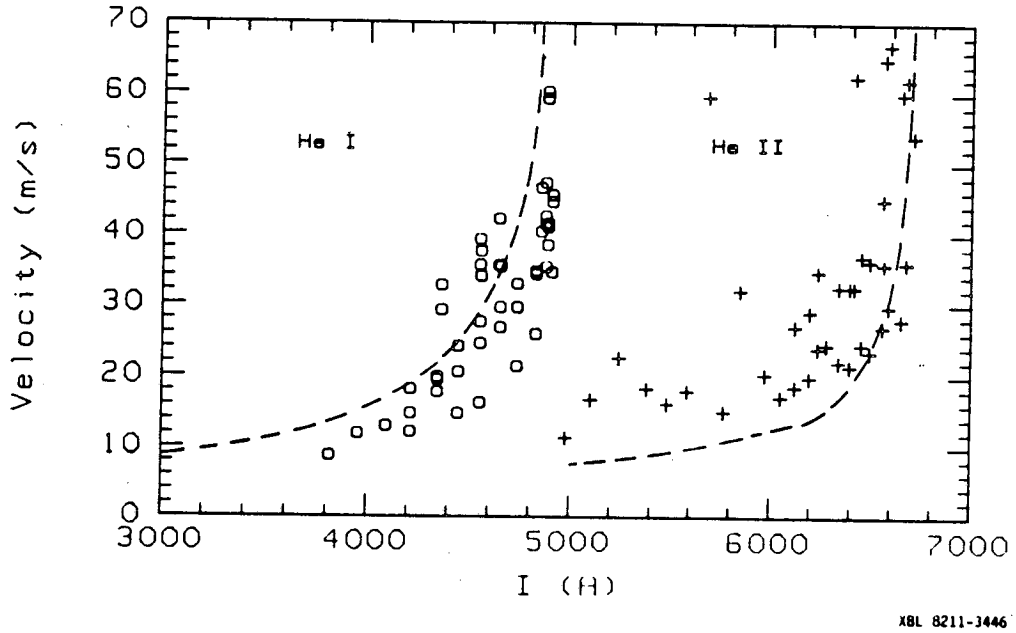

Fig. 8a. Axial quench propagation velocity in D-7H as a function of quench current. The dashed lines are calculated with the program QUENCH.

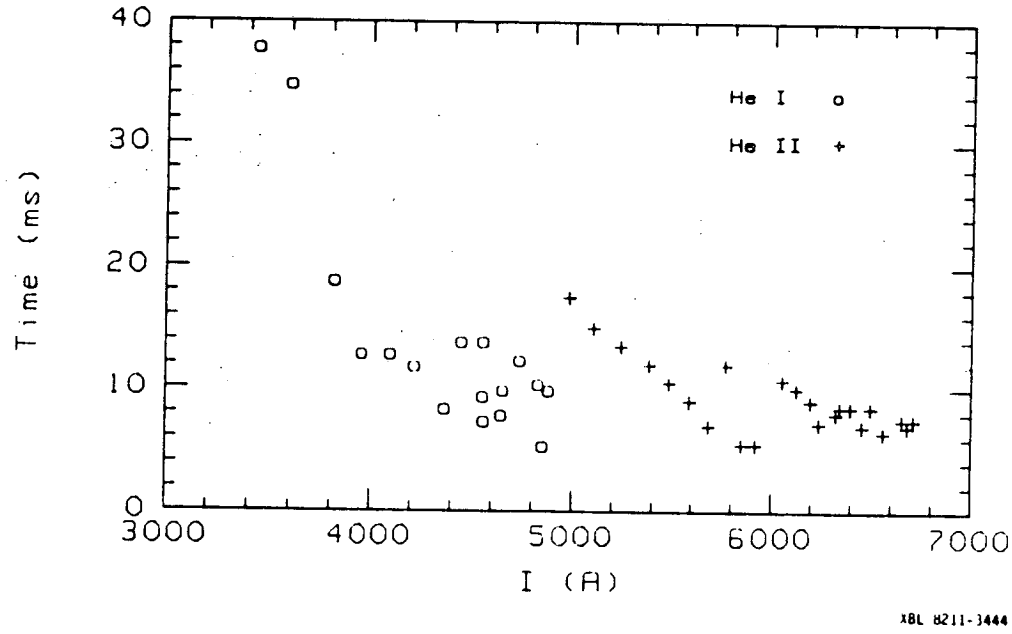

Fig. 8b. Transverse quench propagation: transit time from 1st to 2nd turn vs. current.

The thermal conductivity and the interface effects of the insulation are easy to determine quantitatively whereas the consequences of helium in the winding are hard to evaluate exactly. The quench propagation velocity depends on k. Thus the relative velocities are given by:

$$\frac{V_\perp}{V_q} \propto \sqrt{k_\perp / k_q}$$

Since $k \approx 10^{-4} k_q$

$$\frac{V_\perp}{V_q} \approx 0.01 \ .$$

As shown in Fig. 8, for the model dipole, the transverse propagation velocity was about 0.7% of the axial propagation velocity.

More detailed discussions of quench in superconducting coils are given in the references.

Protection

The protection of a superconducting coil depends on many factors including quench velocity. This dependence is not simple, however. The most relevant parameter for coil protection, assuming voltages are low enough that no arcing occurs, is the ultimate temperature reached in the coil. If this is less than about 400 or 500K then few adverse effects are possible. When higher temperatures are reached parts of the insulator can be destroyed, or solder in the conductor may melt.

The conductor temperature is determined by the energy stored in the coil and the physical characteristics of the coil materials such as

specific heat and resistivity. As the coil begins to go normal, the local temperature change is given by

$$\frac{\Delta t}{C} = J^2 \rho \Delta t$$

Both ρ and C depend explicitly on the temperature, so the local temperature is given by the relationship

$$\int_{T_B}^{T} \frac{dT}{C\rho} = \int_0^t J^2 \, dt$$

Because it is the final temperature that is of interest, this process is generally simplified by setting limits on the expression $\int_0^t I^2 dt$ where I is the current in the conductor rather than the current density.

Using the Fermilab Doubler magnets as an example, the left hand integral between 4 and 500K is about 5×10^6 A^2s (sometimes referred to as 5MIITS). If we assume the current decays as an exponential, $I \propto e^{-t/\tau}$, then

$$\int_0^t I^2 \, dt = \int_0^t I_o^2 \, e^{-2t/\tau} dt = \frac{\tau}{2} I_o^2$$

Since the current is initially about 4000A, the acceptable time constant for discharge of the Doubler coils is about 1/2 second. Of course the decay of the current does not follow a perfect exponential,

but the approximation is good enough to give us some insight into the requirements on quench detection and coil protection.

Several approaches can be used to protect a high current density superconducting coil.

1. The quench propagation velocities, axial and transverse, can be made so high that enough of the coil is normal for the coil to self protect, $L/R_{eff} < \tau$, where R_{eff} is the effective (average) resistance of the coil during the discharge. This approach is used in the CBA accelerator.

If the intrinsic quench velocity is not fast enough, the coil may still be protected with a modification of this technique that includes the addition of a heater which is triggered by the detection of a normal region, as done in the Fermilab doubler magnets.

2. Another protection scheme involves an external dump resistor. When a quench is observed the coil can be rapidly discharged through the resistor as shown in the schematics, Figs. 9 and 10.

In either of these circuits the coil is protected if the sum of the delay time, t_d, which is the unavoidable delay between quench initiation and the transfer of current into the dump resistor, and the characteristic decay time, L/R, are less than τ_a the acceptable decay time:

$$t_d + L/R < \tau_a$$

generally $t_d \approx 0.05$ to 0.10s.

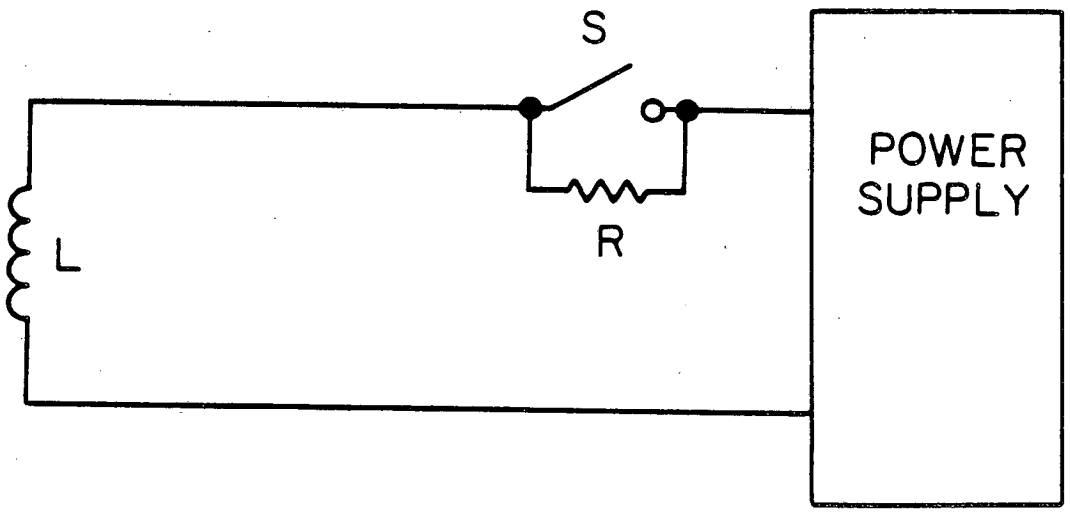

XBL 836-10133

Fig. 9 A protection circuit using an external dump resistor. When a normal region is detected the switch S is opened and the power supply voltage is reduced to zero or reversed.

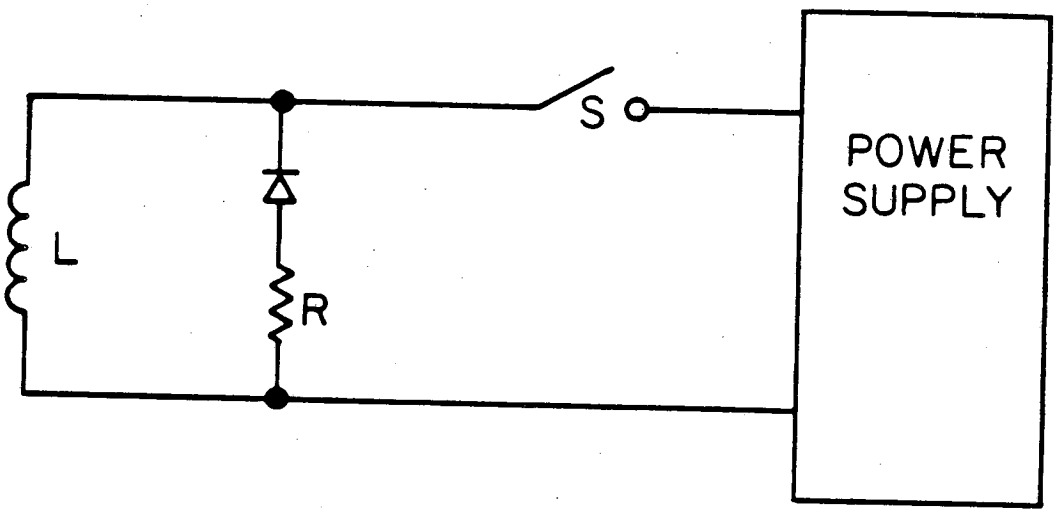

XBL 836-10130

Fig. 10. A different protection circuit using an external dump resistor. When a normal region is observed the switch S is opened and the current flows through the resistor and diode.

3. The coil can be protected by having an inductivity coupled electrical circuit that can accept some of the stored energy. An example is shown in Fig. 11.

The switch S_2 may or may not be in the circuit, but, in either case, as the current begins to decrease in the primary, L_1, after S_1 is opened, the current in L_2 increases and energy is deposited in R_2. This resistance and the coil L_2 may be one and the same. Also the elements S_1 and R_1 may or may not be part of the circuit. A modification of this technique is to have the secondary L_2 closely coupled electrically and magnetically to the coil L_1 and to use the heat generated in the normal coil L_2 to drive a major portion of the superconducting coil L_1 normal.

4. As mentioned above, a coil can be self protected if the quench propagation velocity is fast enough. A method of increasing the quench propagation velocity is to introduce a current pulse that causes the current in all or part of the coil to increase quickly to a value higher than the critical current. This pulse can be accomplished by means of a capacitive dump. Several circuits are possible, and one is shown in Fig. 12. The value of C must be chosen to give a short but high-current pulse into the section of the coil, L', which is best accomplished if L' is small and C is large.

A slight modification of this approach is to have a coil wound with two conductors in parallel with very small mutual inductance. Then a capacitor is discharged across one circuit driving it normal very quickly. The transient current increase in one conductor is

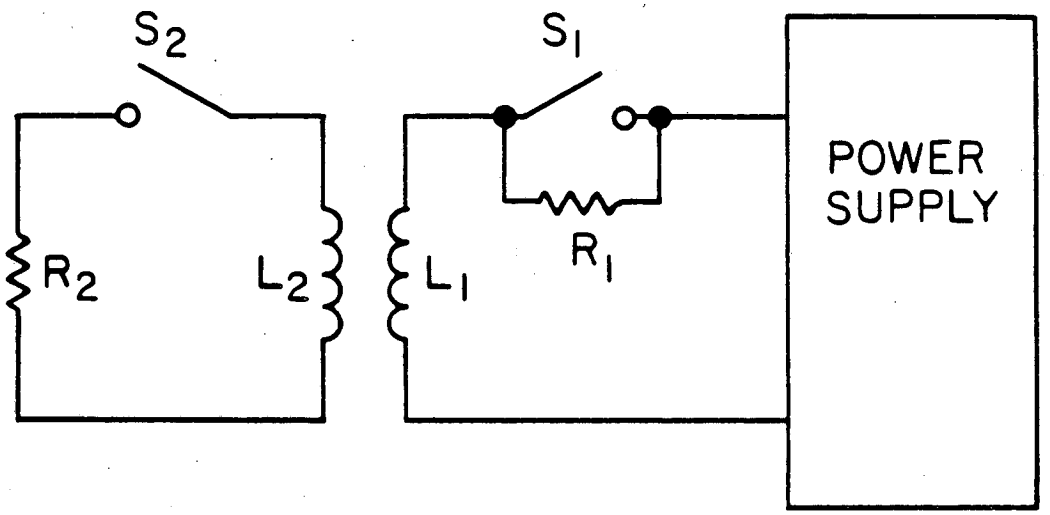

Fig. 11. A protection circuit in which the coil L_1 is discharged through an inductivily coupled resistor R_2. Addition protection can be supplied by having a resistor R_1 in the circuit as shown in Fig. 9.

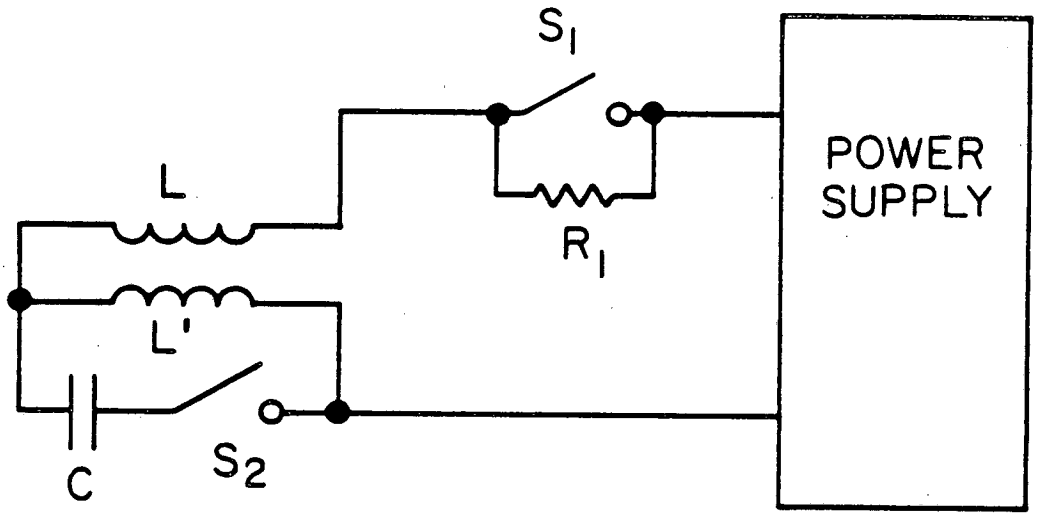

XBL 836-10132

Fig. 12. A protection circuit that combines the features of Fig. 9 and pulsed discharge into part of the circuit. Depending on the polarity of the capacitor section L or L' will be quenched when the capacitor is discharged.

counter-balanced by a current decrease in the other. The heating in the one section then causes the other to be driven normal. All of the coil may or may not go normal, but the quench, once started by the voltage and current transient, will then propagate through the coil.

V. COIL STRESSES

Mechanical stress developed within the windings and in the structural material around the windings of a superconducting coil is generally very high to minimize material costs. As mechanical limits are approached, accurate prediction of stresses is required, necessitating complex analysis and measurements that are difficult, especially at low temperatures. However, we can calculate approximate stresses from very simple models that represent a highly idealized magnet. The following results have been found to be useful:

The idealized coil has winding layers bounded by concentric circles as shown in Fig. 13; the current density per unit circumference varies as $J = J_0 \cos\theta$, independent of radius. We call this an ICT (Idealized Cosine Theta) coil. If the coil thickness h is small compared to its radius (a "thin" ICT coil) the central field is

$$B_0 = (1/2)\ \mu_0\ J_0 h\left[1 + (a/b)^2\right]$$

The Lorentz body forces per unit length x circumference(N/m^2)are:

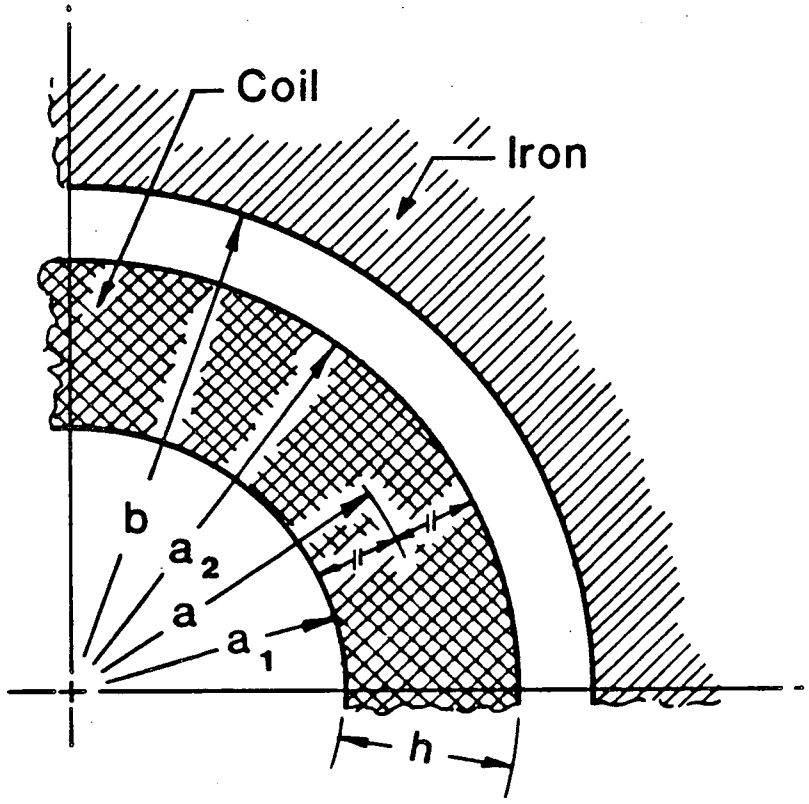

Fig. 13. Nomenclature for coils.

$$f_t = -(1/4)\ \mu_0\ (J_0 h)^2\ a\left[1 + (a/b)^2\right] \sin 2\theta$$

$$f_r = (1/4)\ \mu_0\ (J_0 h)^2\ a\ (a/b)^2\ (1 + \cos 2\theta)$$

The circumferential compressive pressure p_t and the radial pressure p_r acting outward (N/m^2) are:

$$p_t = (1/8)\ \mu_0\ (J_0 h)^2\ (a/h)\ \left[1 + (a/b)^2\right]\ (1 + \cos 2\theta)\ ,$$

$$p_r = (1/8)\ \mu_0\ (J_0 h)^2\ \left[1 + 3(a/b)^2\right]\ (1 + \cos 2\theta)$$

where the radial outward pressure is due to both the local radial body force and the accumulated tangential pressure.

For a "thick" ICT coil, the circumferential and radial pressures again vary as $1 + \cos 2\theta$. The thick-coil results are shown in Fig. 14 in comparison with those for the thin ICT coil of radius $a = (1/2)(a_1 + a_2)$ that produces the same aperture field. Fig. 14a shows how the total radial force at radius a_2 and the total circumferential force at $\Theta = 0$ are affected by coil thickness and iron radius. Fig. 14b shows how the variation of circumferential stress through the thickness of the coil is affected by coil thickness and iron radius.

Two more realistic coils are represented in Figs. 15a and 15b. We will refer to these as the "layer-" and "block-type" coils, often referred to as "intersecting ellipse" and "cosine theta" coils respectively.

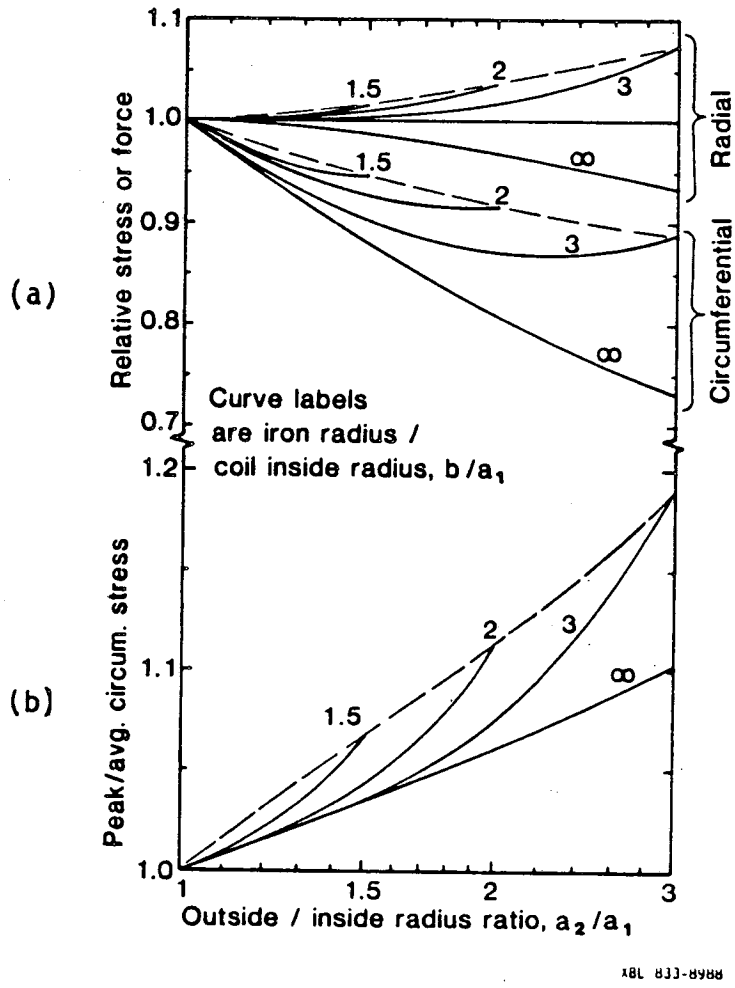

Fig. 14. Thick cos θ coil. Upper curves are max. radial stress on outside of coil and total circum. force normalized to values for thin coil producing same field. Lower curves are peak-to-average circum. stress ratio.

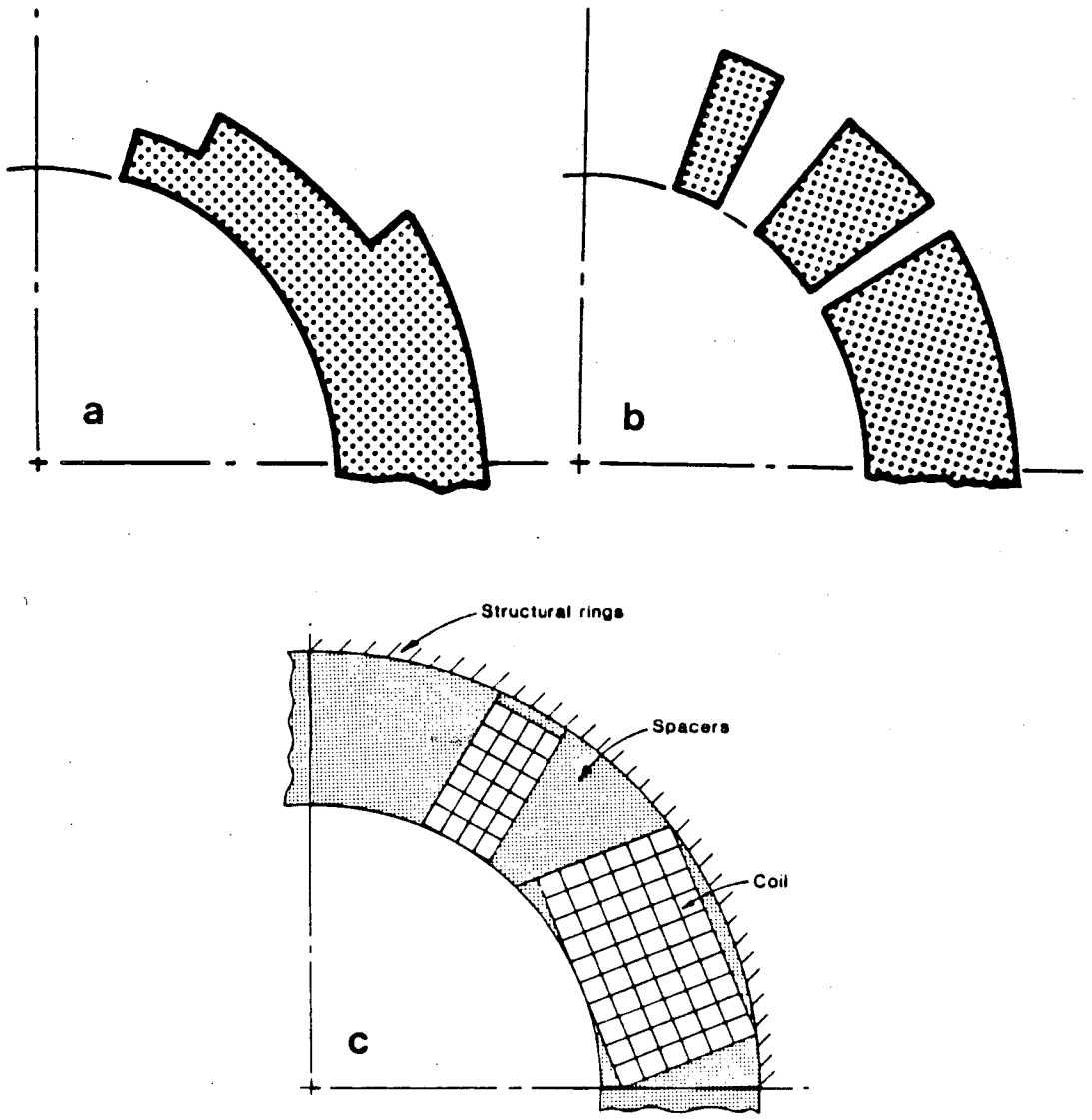

XBL 833-8987A

Fig. 15. Coil cross sections: (a) layer type; (b) block type; (c) rectangular-block type.

These two coil configurations have been analyzed for a wide range of parameters: One through three blocks or layers, coil radius ratios (a_2/a_1) of 1.5 and 2.0, and for both close-fitting iron and no iron. The total radial and circumferential forces have been compared with those for thick ICT coils that produce the same aperture field. For the one-block or one-layer coils, which are identical, the sc differences are at most 15 percent. For two or more layers or blocks the differences are 7 percent or less.

The outside radial pressure distributions only roughly approximate those of the ICT coil as shown in Fig. 16. For the block-type coils, the circumferential pressure distributions are indistinguishable from those for the equivalent ICT coils. For the layer-type magnet, the circumferential stress, Fig. 17, in the innermost layers is substantially greater because those layers carry more current.

A third family of coils, Fig. 15c, which bear little resemblance to the ICT coil, has been investigated along with the surrounding ring structure. The distribution of circumferential stresses within each block is similar to that for the ICT coil. The radial forces are extremely irregular, there being large concentrated loads at each wedge-shaped spacer. For only a single current "block" the total circumferential force is 20 to 25 percent lower than that for the equivalent thick ICT coil, depending on the iron radius, the maximum bending moment in the ring is 10 to 26 percent greater, and the maximum displacement of the ring is 4 to 8 percent greater. These differences decrease rapidly as the number of blocks increases; all are less than 7 percent for three blocks.

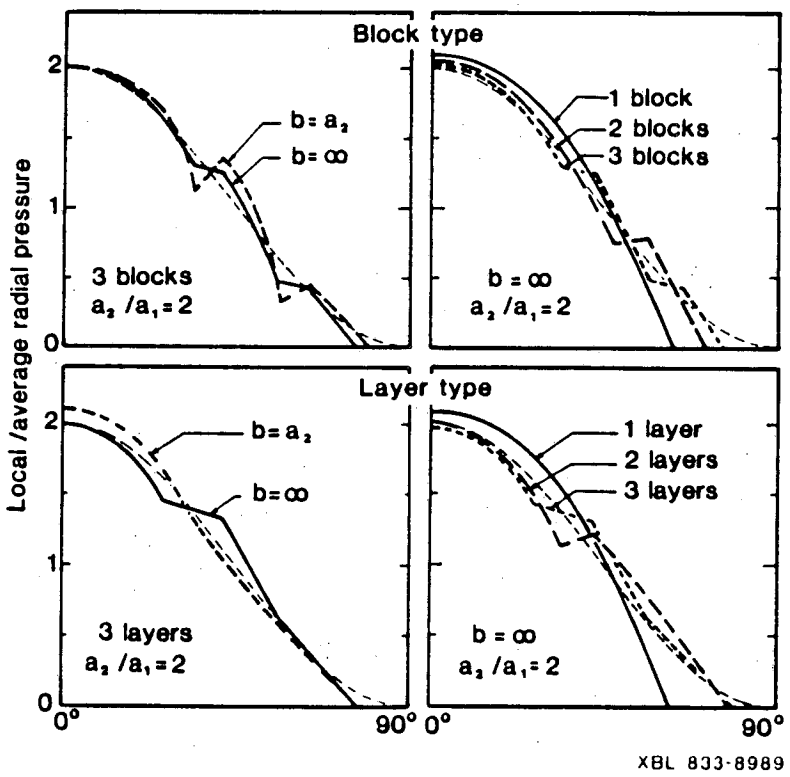

Fig. 16. Block- and layer-type coils; radial pressure distribution on outside: effects of iron radius, and number of blocks or layers.

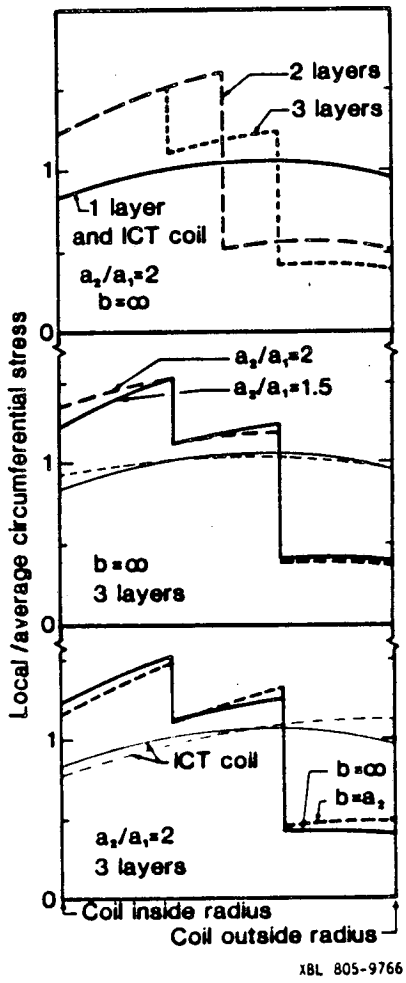

Fig. 17. Layer-type coils: circumferential stress distribution at $\theta = 0$, effects of number of layers, coil thickness, and iron radius.

VI. SUPPORTING STRUCTURE STRESS AND DEFLECTION

We present in turn: results for a thin, uniform, circular ring with the simplest possible radial load distribution; results for a thin ring with more complex loading, and results for a thick circular ring of uniform cross section with simple loading. All are based on an exact solution of the equations of the Theory of Elasticity.

The loading produced by an ICT coil is of the form $p = p_0 \cos 2\theta + p_1$ (N/m^2). The resulting internal forces and the displacements depicted in Fig. 18 for a thin, uniform ring are:

Bending moment (N)	$M = -(1/3)\, p_0\, a^2 \cos 2\theta$
Hoop tension (N/m)	$T = -(1/3)\, p_0\, a \cos 2\theta + p_1\, a$
Radial shear (N/m)	$V = (2/3)\, p_0\, a \sin 2\theta$
Radial displacement:	$u = u_0 \cos 2\theta$, where $u_0 = p_0\, a^4/(9\, E\, I)$
Circumferential displacement:	$v = -(u_0/2) \sin 2\theta$

M, T, and V are per unit axial length, a is the ring radius (m), I is the moment of inertia of the ring cross section per unit axial length (m^3), and E is the elastic modulus (N/m^2).

But the loading produced by real coils is not the smooth loading produced by the ICT coil. For example, in the block coil of Fig. 15c the radial loading on the spacer is much greater than in this region on a ICT coil because of the direction of the compressive loads at each side of the spacer. To determine the effect of the irregularity of the loading, we considered the effect of a set of concentrated loads that approximate a continuous $1 + \cos 2\theta$ loading. For two loads, the

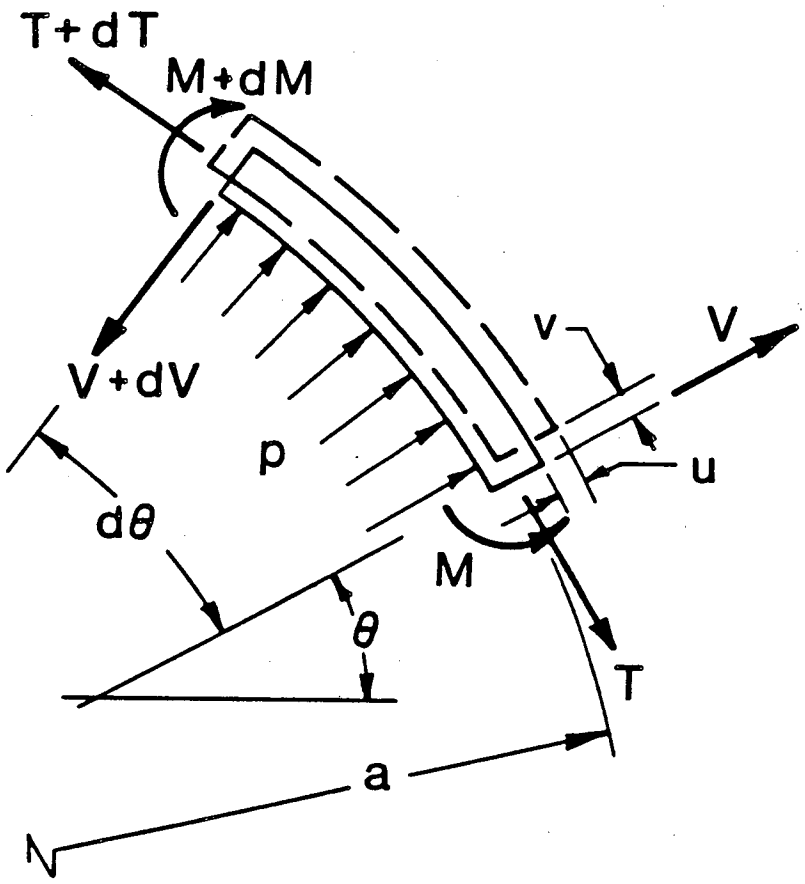

XBL 805-9765

Fig. 18. Nomenclature for thin rings.

maximum bending moment and displacement are 10 percent higher than for the continuous case. Each doubling of the number of loads was found to reduce the difference to 1/4 of its previous value (thus 10% → 25% → 0.6%).

An exact solution of the equations of elasticity theory for a thick ring with surface pressure and shear forces is available. For a loading, $p = p_o \cos 2\theta + p_1$ on the inside surface the relevant stresses and displacements are expressed by the following formulas:

$$\sigma_{t,in} = - 2 K_1 p_o (a_1/h)^2 \cos 2\theta + K_5 p_1 (a_1/h)$$

$$\sigma_{t,out} = + 2 K_2 p_o (a_1/h)^2 \cos 2\theta + p_1 (a_1/h)/K_6$$

$$\tau_{max} = K_3 p_o (a_1/h) \sin 2\theta$$

$$u = \frac{4}{3} K_4 \frac{p_o a_1 (a_1/h)^3}{E} \cos 2\theta + K_7 \frac{p_1 a_1 (a_1/h)}{E}$$

$$v = - \frac{2}{3} K_4 \frac{p_o a_1 (a_1/h)^3}{E} \sin 2\theta$$

The K-factors are presented in Fig. 19. Depending on the relative magnitudes of the p_o and p_1 terms, the maximum circumferential stress can occur at either the inside or outside surface at either the $\theta = 0$ or 90° positions.

With the exception of the circumferential stresses in the layer-type coils and the radial forces produced by the one-block coils, the

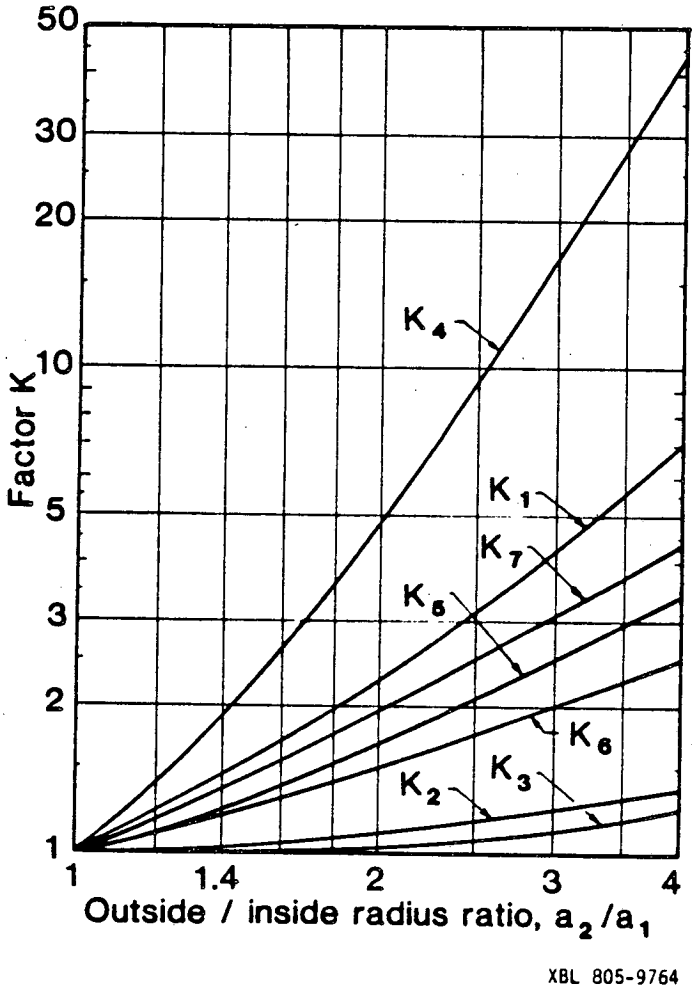

Fig. 19. Thick ring: factors for stresses and displacements.

stresses and displacements of the more realistic coils are closely approximated by those of the idealized cosine theta configuration.

VII. POSSIBLE DIPOLE MAGNET CONFIGURATIONS*

We present here a collection of dipole magnet cross sections together with a partial description of how they are related geometrically. The relationships indicated do not necessarily imply the actual historical or evolutionary path of development. Because higher multipole fields are often required in accelerators, brief consideration is given to cross sections of magnets of higher multipole order.

The magnets under consideration (Fig. 20) have currents parallel to the axis except at the ends, and are long. The relationship between current distribution and magnetic field is essentially two dimensional. The coils are usually surrounded by an iron yoke, but the emphasis is on conductor-dominated configurations capable of producing a rather uniform magnetic field in the aperture; the iron usually has a small effect.

Most of the cross-section sketches show only the first quadrant; the entire cross sections include reflections into the other three quadrants with currents in the senses +,-,-,+, perpendicular to the plane of the cross section, in quadrants 1 through 4, respectively. The iron yoke is shown (represented by its inner boundary) only for those configurations where the iron is an essential part of the design or

*An excerpt from R.B. Meuser, Structural Analysis of Superconducting Bending Magnets, LBL-10950, Lawrence Berkeley Laboratory.

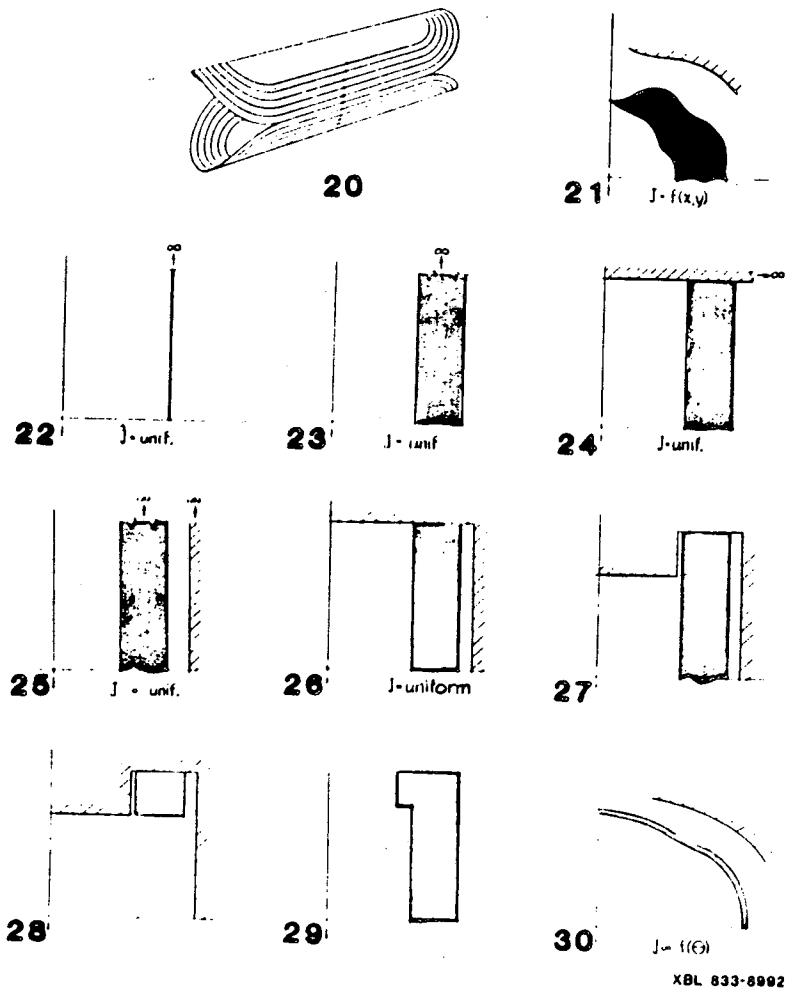

Fig. 20. A sketch of the general shape of the windings for a superconducting dipole.

Figs. 21–48. Cross sections of windings for accelerator dipoles. The details of each configuration are described in the text.

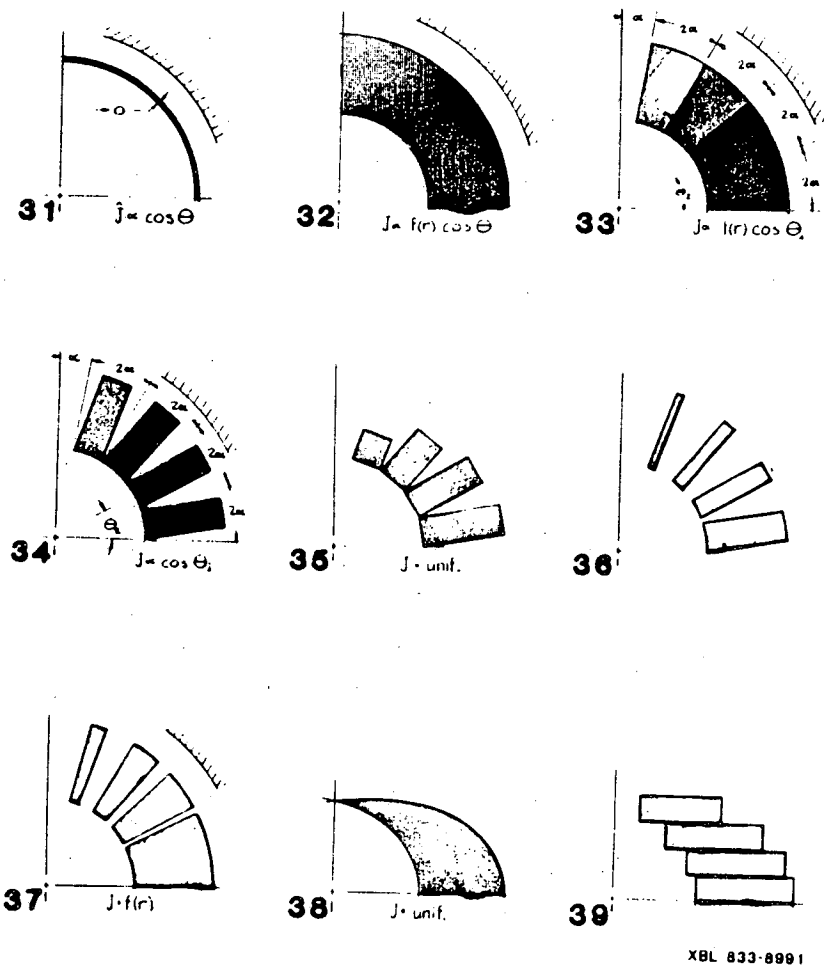

Figs. 21-48. Cross sections of windings for accelerator dipoles. The details of each configuration are described in the text.

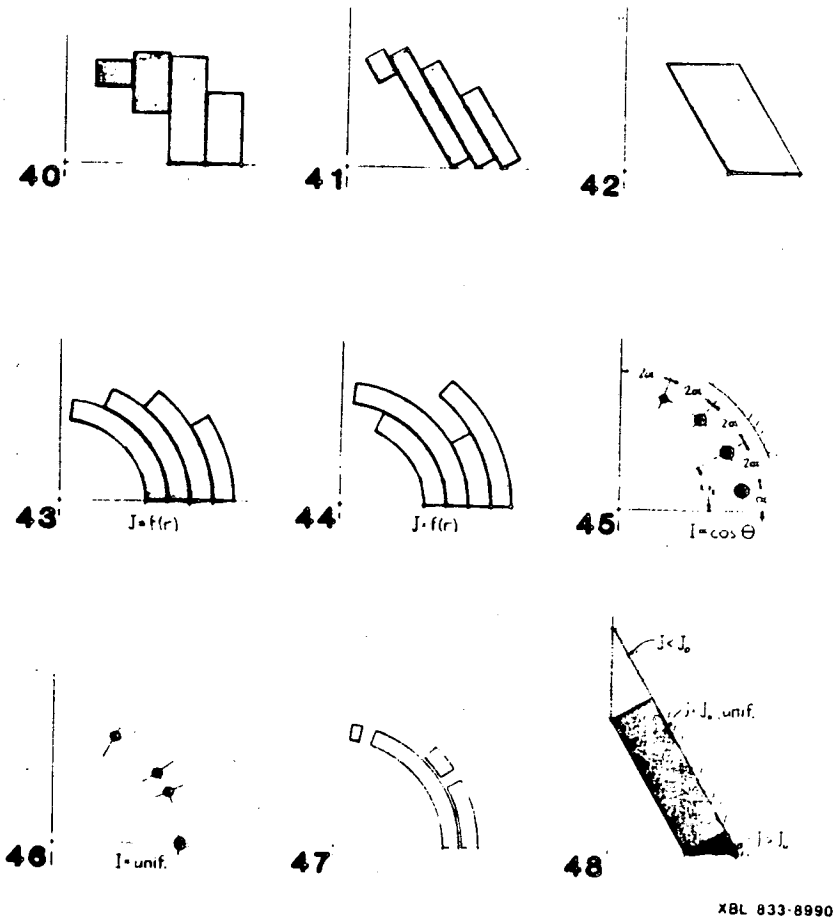

Figs. 21–48. Cross sections of windings for accelerator dipoles. The details of each configuration are described in the text.

where the optimized coil configuration is independent of the iron. The outer iron boundary can be assymetrical.

In concentrating our attention on the cross section we necessarily ignore the practical matter of the design and construction of the ends, which is where many of the problems lie. And too, we carefully sidestep consideration of iron-saturation effects, important as they are, and of the virtues of one configuration compared with those of another.

Only a few references are presented; the list is far from complete. A cited reference does not necessarily represent the invention or first use of a particular configuration.

Configuration

The most general configuration, of which all of the other configurations are simply special cases, is illustrated in Fig. 21. In principle one can choose almost any shapes for the coil inner and outer boundaries and the iron boundary, and then find a current density distribution that produces a uniform field in the aperture. If one choses circles for these boundaries, for example, then one current density distribution (not the only one, incidentally) that produces a uniform field is $J = J_0 f(r) \cos\theta$, where J_0 is a constant, and $f(r)$ is any function of r.

The simplest configuration (Fig. 22) consists of a pair of current sheets, with opposite currents, extending to infinity. With uniform lineal current density, a uniform field is produced in the region between the two sheets. The sheets can become infinite in thickness by superposition (Fig. 23). To overcome the practical nuisance of coils extending to infinity, the coil can be cut off and iron reflectors added

above and below the aperture (Fig. 24). With the further addition of iron at the sides (Fig. 25), the current-sheet pair evolves into the familiar "picture frame" (or is it "window frame"?) configuration (Fig. 26). Addition of pole tips (Fig. 27) increases the field strength, and removal of part of the coil near the horizontal axis (Fig. 28) permits the use of flat coils. However, both of these modifications destroy the uniformity of the field.

If the coil is cut off at some point and iron reflectors are not added, the field uniformity is destroyed. But part of the loss of uniformity can be recaptured by adding current lumps at the extremities of the coil (Fig. 29). By further refinements of the coil shape the configurations could evolve into some of the more complex ones considered later.

The general configuration of Fig. 21 can be specialized somewhat to a thin coil of arbitrary shape (Fig. 30) and further to a thin circular coil (Fig. 31), in which case a uniform field is produced in the aperture if the linear current censity in the coil varies as $\cos\theta$. The thin shell can be made thick by superposition, with the current density a function of r (Fig. 32).

A continuous azimuthal variation of current density cannot be achieved in practice, and so a number of approximations have been invented. One such configuration, (Beth, Ref. 5), is shown in Fig. 33. The current density within each region is uniform in θ. If the number of regions is N, then $2N-1$ higher-order multipole coefficients can be made exactly zero. If the inner and outer boundaries of the coil are circular, then the only kind of radial variation of current density that can be readily achieved in a superconducting magnet, either by tapering

the conductor radially or by inserting wedge-shaped spacers between the turns, is an inverse variation ($f(r) = 1/r$). For a homogeneous, resistive conductor of keystone-shaped cross section, the current density could be uniform. But for a twisted cable flattened to a keystone cross-section, as used in some superconducting coils, the macroscopic current density varies inversely with radius.

By making the sides of the current "blocks" parallel (Fig. 34) to accommodate conductors of rectangular cross section, one achieves a current density that varies inversely with radius in an overall sense, while the current density in the region is uniform. The Beth prescription demands that the current density in each region be proportional to the angle to the centerline of the region. The average, current density in a block can be varied by varying the number of conductors and replacing the missing conductors with spacers. But it is not possible to satisfy Beth's prescription for current density exactly if only one kind of conductor is used throughout. So, in practice, one makes the current density approximate the Beth prescription, then juggles the angular positions of the boundaries to get the best field quality. The original BNL Isabelle magnets were close approximations to the kind shown in Fig. 34.

To achieve a practical approximation to Beth's prescription in a different way, the current blocks can all have the same current density, but the sizes of the blocks can be varied by varying either the depth (Fig. 35) or width (Fig. 36) of the block. Again, the angular positions of the blocks are adjusted to produce the best field quality.

In another sort of approximation to a $\cos\theta$ coil (Fig. 37) (Halbach, Ref. 6), the current density is uniform in azimuth within each

current block, but the azimuthal positions of the block sides are adjusted to produce the best field quality.

If two elliptical regions having uniform current densities in opposing senses are superimposed, leaving a zero-current hole in the region of overlap, then provided the ellipses have the same aspects ratios the field in the hole is uniform. This result is true even if the ellipses are not equal in size. In a magnet the net current must be zero, so the two ellipses must be equal (Fig. 38). The central region in this figure appears to be a circle, but it is in fact the boundary of the two intersecting ellipses. A specialization is the classical overlapping circle configuration (Rabi, 1934, Ref. 7). Various practical approximations to the intersecting ellipse geometry have been used or proposed involving horizontal conductor layers (Fig. 39), vertical layers (Fig. 40), flat layers set at an angle (Fig. 41), which is specialized to that in (Fig. 42), and cylindrical layers (Fig. 43). The configuration involving cylindrical layers (Fig. 43) is commonly referred to as an "intersecting ellipse" magnet. But the order of the layers can be inverted or scrambled (Fig. 44) in which case the nomenclature becomes severely strained. Thin coils, at least, of this sort might equally well be called "cosine theta" coils; the conductor density per unit angle indeed varies as a stepwise approximation to $\cos\theta$.

Various arrangements of single conductors or small bundles of conductors that produce rather uniform fields can be devised. The one shown in Fig. 45 stems directly from the Beth design (Fig. 34), and the same number of higher order multipole coefficients are zero; the magnitudes of the non-zero ones are larger than for the Beth design, however.

The one in Fig. 46 (Rechen, Ref. 8) involves conductors having equal currents. For the configuration shown, three higher-order multipoles are exactly zero. If a different criterion for field uniformity is used, presumable a more cosine-like distribution of conductors could be obtained.

Many of the designs illustrated can be improved, as regards field uniformity, by increasing the number of "layers" or "blocks" of conductors, but often this is not feasible or is costly. Another method that sometimes works is to add spacers, which effectively increases the number of "degrees of freedom" of the design. On illustration is the configuration boundary, designed by Palmer (Fig. 47, Ref. 9) as the alternative design for the Isabelle magnets.

A configuration that appears to have come about by the process of spontaneous creation, defying any conceivable path of evolution from simpler forms, is illustrated in Fig. 48 (Ref. 10). (Assymmetrical forms are also considered in the reference, which incidentally is a rather snazzy piece of work.) The sides can be at any angle. The current density in the corner regions is different from that in the flat sides. In particular, if the angle is 45°, then the current density in the top corner is zero, and that in the side pockets is twice that in the sloping sides. The field at the iron surface can be made as small a fraction of the field in the aperture as desired by thickening the coil, but that increases the quantity of conductor required, perhaps intolerably. Despite some practical problems, the design stands almost alone, accompanied only the window frame configuration, among the configurations considered here, that not only creates an absolutely uniform magnetic field but also can be built at all.

Most of the designs illustrated can be transposed into magnets of higher multiple order. For iron-free magnets, or magnets having a circular iron boundary, if the angular position of each infinitesimal element is halved, and the number of quadrants (now "octants") is doubled, then a quadrupole magnet is produced. This is only practical when the configuration is basically cylindrical.

APPENDIX

I. Superconducting Materials

Three superconducting materials are now being considered for accelerator dipoles. The first is Nb-Ti, a ductile alloy, that has been used in many large magnets and can be used up to about 8T at 4.4K and 10T at 1.8K. The second, Nb-Ti-Ta, is a relative newcomer in terms of commercial availability and promises to extend the performance at 1.8K to about 12T. The third superconductor is Nb_3Sn, which is a brittle compound that may operate effectively at fields as high as 12T at 4.4K. The maximum current densities that these superconductors can carry as a function of field are shown in Fig. 49. To be useful in an accelerator dipole the superconductor must carry about 1000 A/mm^2. The current carrying capacity of the superconductor also depends on the temperature as well as the magnetic field. The surface defining the superconducting region and magnitude of the critical current as a function of both field, current, and temperature was shown in Fig. 1. Though this figure shows that the critical current increases as the temperature drops, the effect is much more pronounced for some materials than others. For example, at 4.4K the critical current of Nb-Ti and Nb-Ti-Ta are about the same, but Nb-Ti-Ta is much better at 1.8K even though Nb-Ti has also improved considerably. On the other hand Nb_3Sn improves some, but very little between 4.4 and 1.8K. Some upper critical fields and upper critical temperatures of superconductors are presented in Table III.

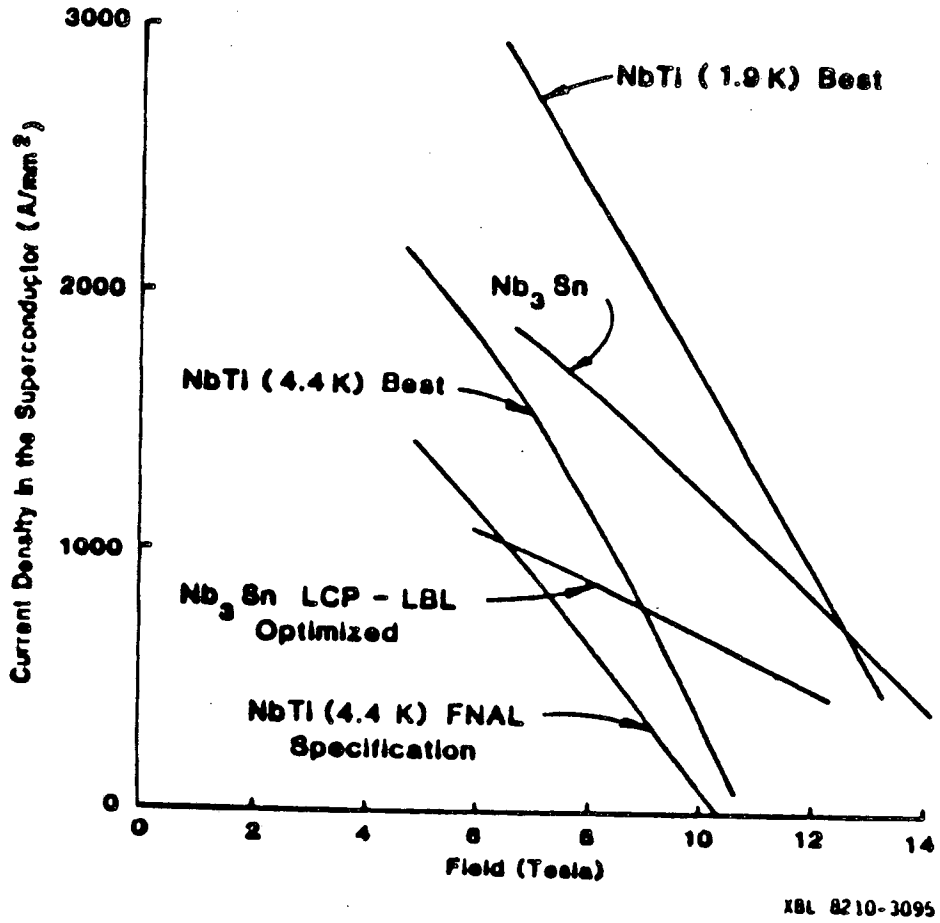

Fig. 49. Critical current density as a function of magnetic field in commercially available superconductors.

TABLE III

Critical Temperatures and Fields of Several Superconductors

Material	T_c (k)	H_c (T)
Nb-Ti	9.5	11
Nb-Zr	10.9	10
Nb_3Sn	18.0	25
Nb_3Ge	23.2	36
V_3Ga	14.8	21
Nb_3Al	18.7	32

II. Conductor Matrix Material

A good normal conductor is placed in contact with the superconductor to carry the current should the superconductor undergo a transition to the normal state. The metals normally used as stabilizers are relatively pure copper and aluminum. The resistivity of pure metals generally decreases as the temperature decreases as shown in Fig. 50. As the temperature drops the resistivity of practical materials appears to reach a lower limit. Typically, the copper used in superconducting magnets is of a type called oxygen free, high conductivity (OFHC). This type of copper is available from several manufacturers, and, in bulk, has a residual resistivity ratio (RRR), ρ_{300K}/ρ_{4K}, of about 300. In the fabricated conductor this ratio is typically between 50 and 100 because of size effects, impurities that have been added during processing, and some work hardening that is produced during the wire drawing process and is not removed by a final heat treatment.

This limit and the temperature at which it is reached depend on the conductor and its purity and hardness as shown in Fig. 51. Impurities and work hardening raise the resistivity. The background magnetic field also effects the resistance. This effect is called magnetoresistance. The magnetoresistance of copper is given in Figs. 52 and 53. The effects of impurities, magnetic field, and work hardening are basically additive. Thus the highest purity material, which is generally the most expensive, is not always used even though the lowest resistance is desirable.

The other stabilizing material that is used occasionally in superconductors is aluminum. Aluminum has several advantages over copper. First, aluminum can be made fairly pure with little difficulty. Thus,

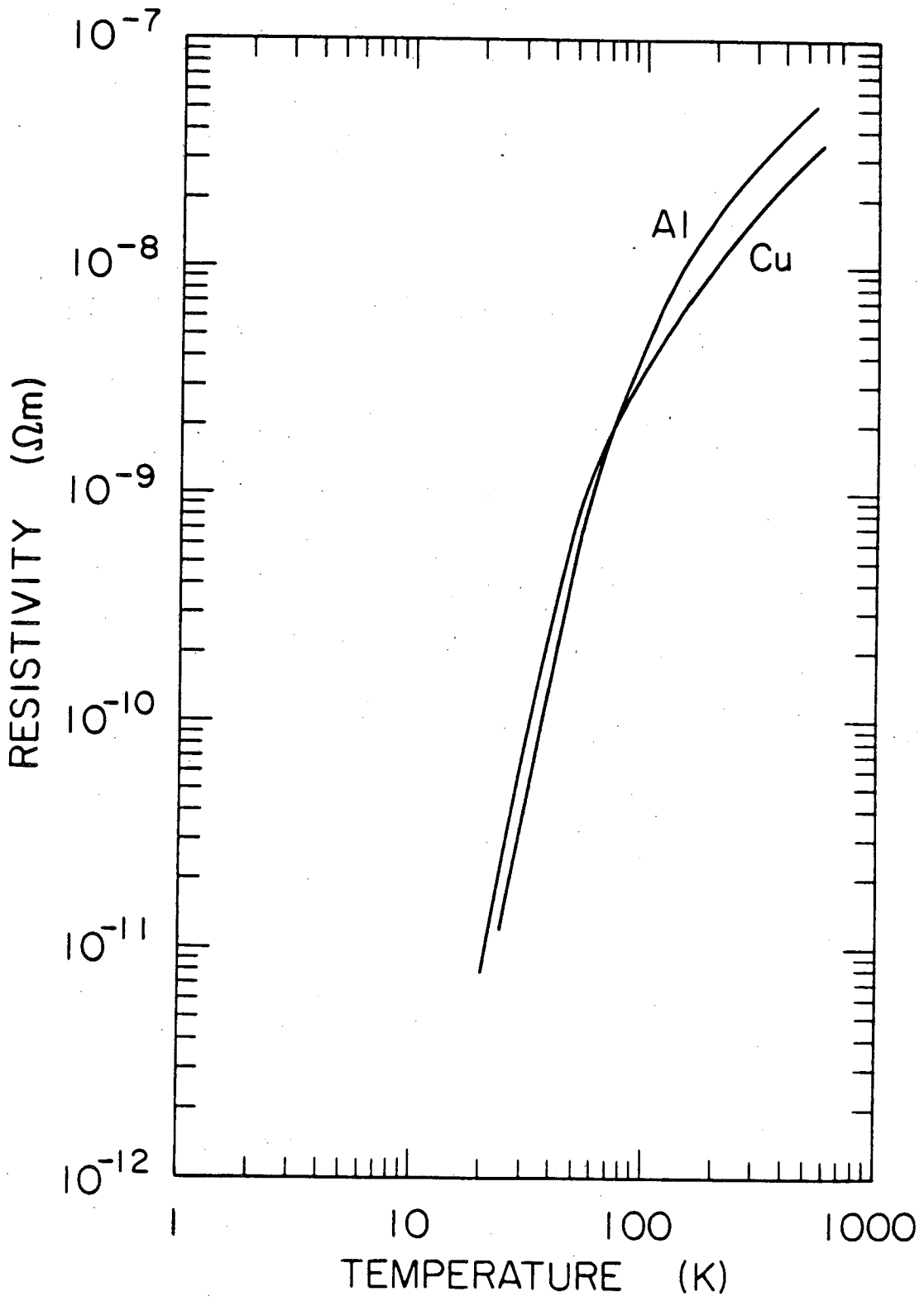

XBL 836-10145

Fig. 50. The resistivity as a function of temperature of pure copper and aluminum.

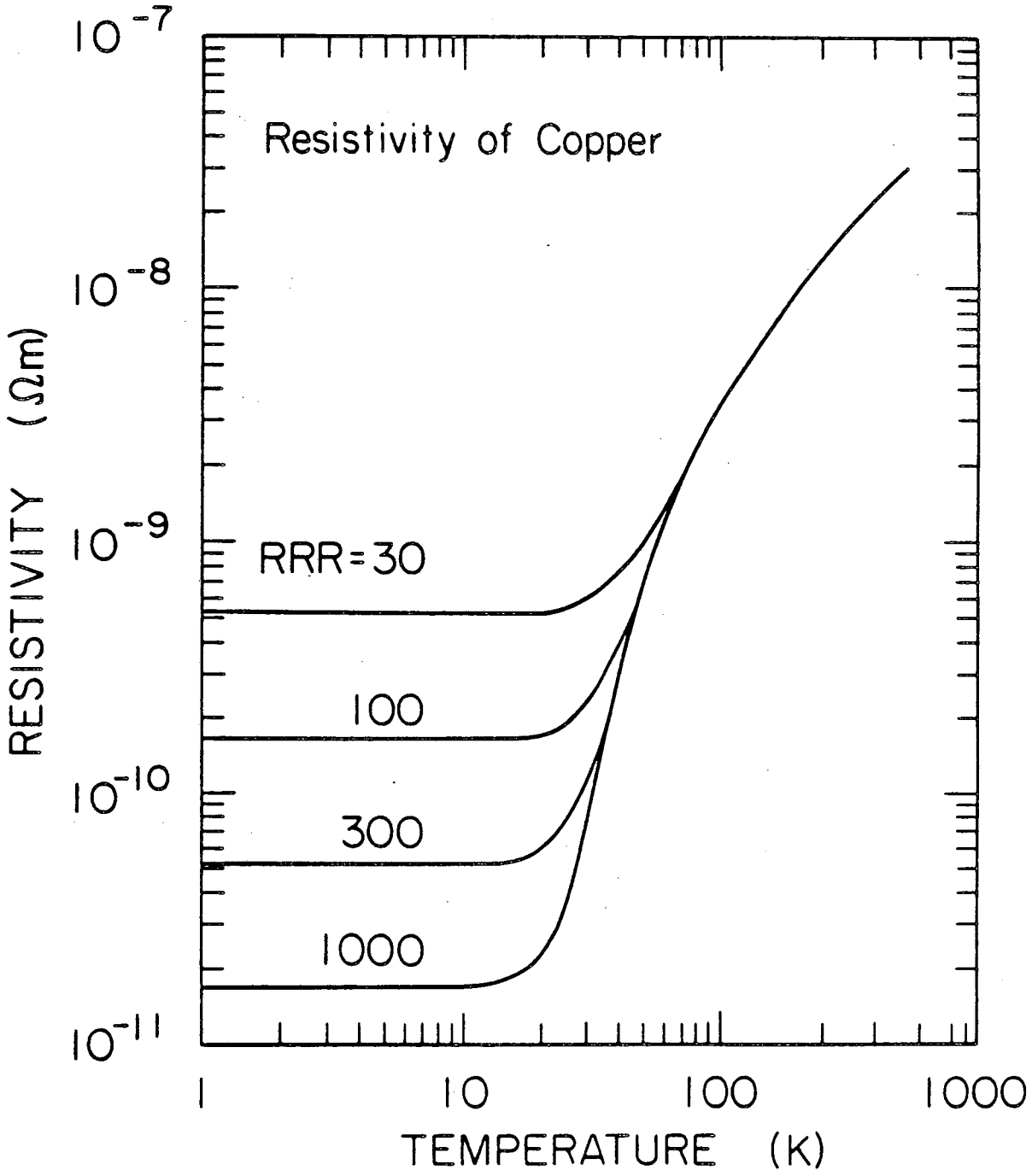

XBL 836-10144

Fig. 51. The resistivity as a function of temperature of copper samples having different resistivity ratio.

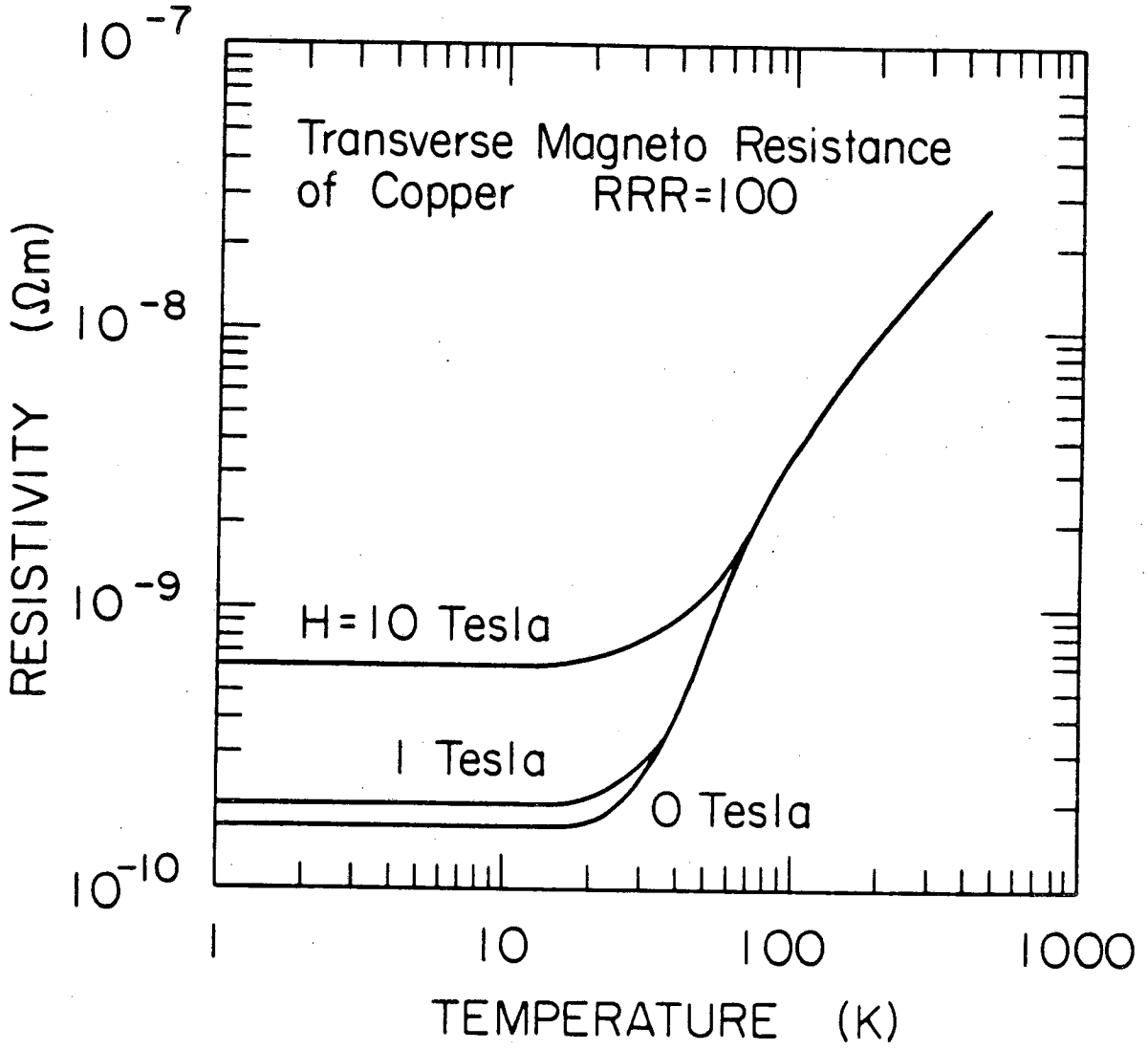

XBL 836-10143

Fig. 52. The temperature dependance of the resistivity of copper in all magnetic fields of 0, 1, and 10 T.

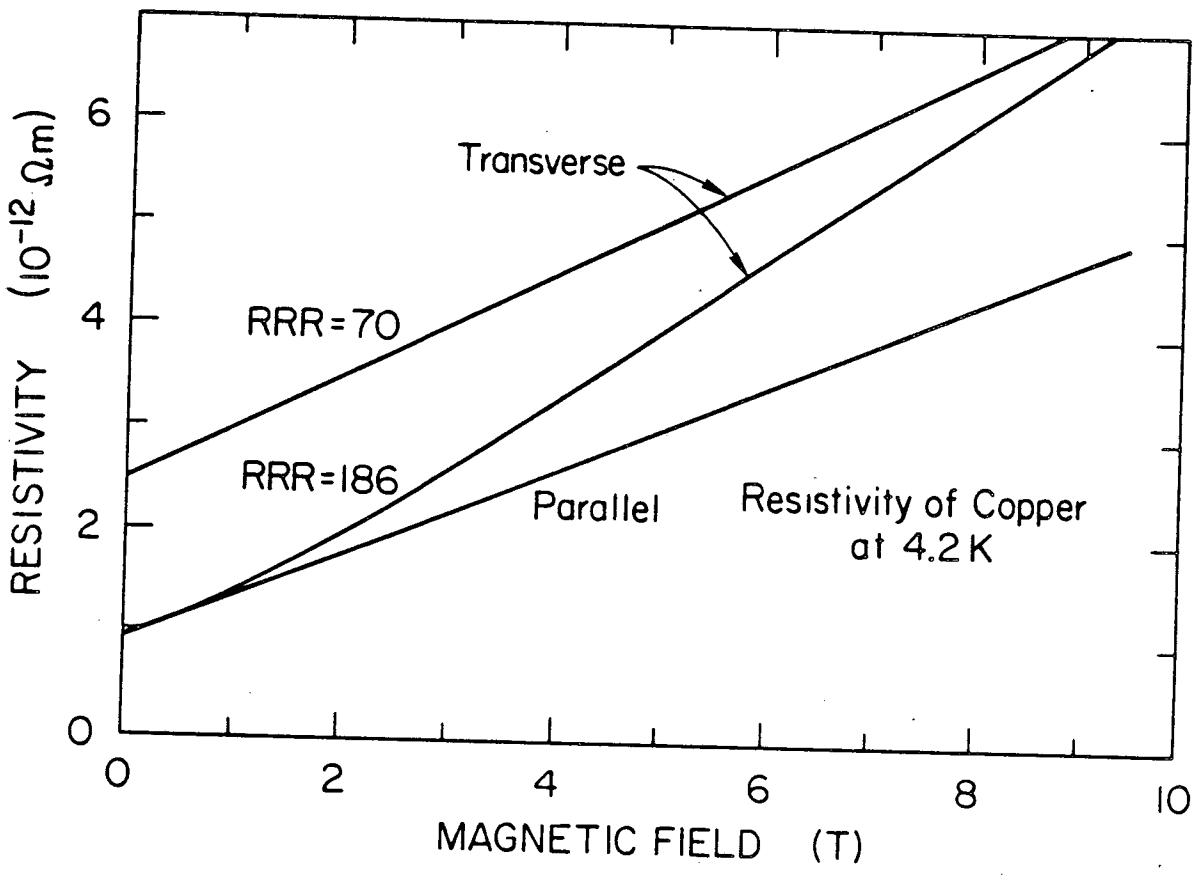

XBL 836-10142

Fig. 53. The resistivity of copper at 4.2K as a function of magnetic field.

though its resistivity is about $2.8 \times 10^{-8}\ \Omega m$ at room temperature compared to $1.8 \times 10^{-8}\ \Omega m$ for copper, resistance ratios of 5000 are fairly easy to achieve and values as high as 50000 have been observed in ultra pure aluminum. Second, because aluminum does not form alloys so easily as other materials and because the annealing temperature of aluminum is low, it is easy to achieve a RRR of 1000 in a magnet. Finally, the magnetoresistivity is much smaller in aluminum than in copper. Which allows it to be a very effective stabilizer at the highest fields.

Aluminum has certain disadvantages, however. The characteristic that makes it easy to purify aluminum also makes it difficult to bond to the superconductor or the copper that is used during superconductor fabrication; and the pure aluminum is so soft that it cannot be used in direct contact with the Nb-Ti during the extrusion and drawing process and must be added later. It is also very difficult to solder to the pure aluminum. Special plating and tinning processes must be used to achieve an adequate bond.

III. Thermal Conductivity

The thermal conductivity k of metals is fairly easily determined from the relationship.

$$k\rho = \frac{L}{T}$$

where ρ is the electrical resistivity, T is the temperature and $L = 2.4 \times 10^{-8} V^2/K^2$ is a constant that is the same for all metals. This formula reflects the fundamental relationship between electrical and

thermal conductivity in metals, which are both determined by the conduction electrons.

The thermal conductivity of other materials, in particular insulators, is not so easily estimated; in fact it must be measured. Some curves of the temperature dependence of k are given in Fig. 54. The thermal conductivity is much lower in the insulators than in the metals. However, the insulators are usually quite thin in regions where the electrical insulation is important and another thermal impedence becomes important. This is the boundary or Kapitza resistance that exist between any two materials and is high between metals and insulators. Assuming good mechanical bonding, epoxy to metal, we find there is a boundary resistance of about $5K/Wcm^2$. For insulation such as a kapton or mylar sheet wrapped around the conductor this boundary effect is much greater than the thermal impedance of the insulator itself. Also, if a thin layer of helium exists between a metal and an insulator this already significant resistance can increase by a factor of 10.

IV. Specific Heat

The specific heat of the components of a coil affect its stability by determining the initial temperature excursion associated with a disturbance. The reason magnets are so sensitive to disturbances is that the specific heat is about a factor of 10^2 to 10^4 smaller at 4K than at 300K. The specific heats of copper and aluminum are given in Fig. 55 and the specific heat of epoxy is given in Fig. 56. The specific heat of a superconductor depends on the superconducting state and the background field.

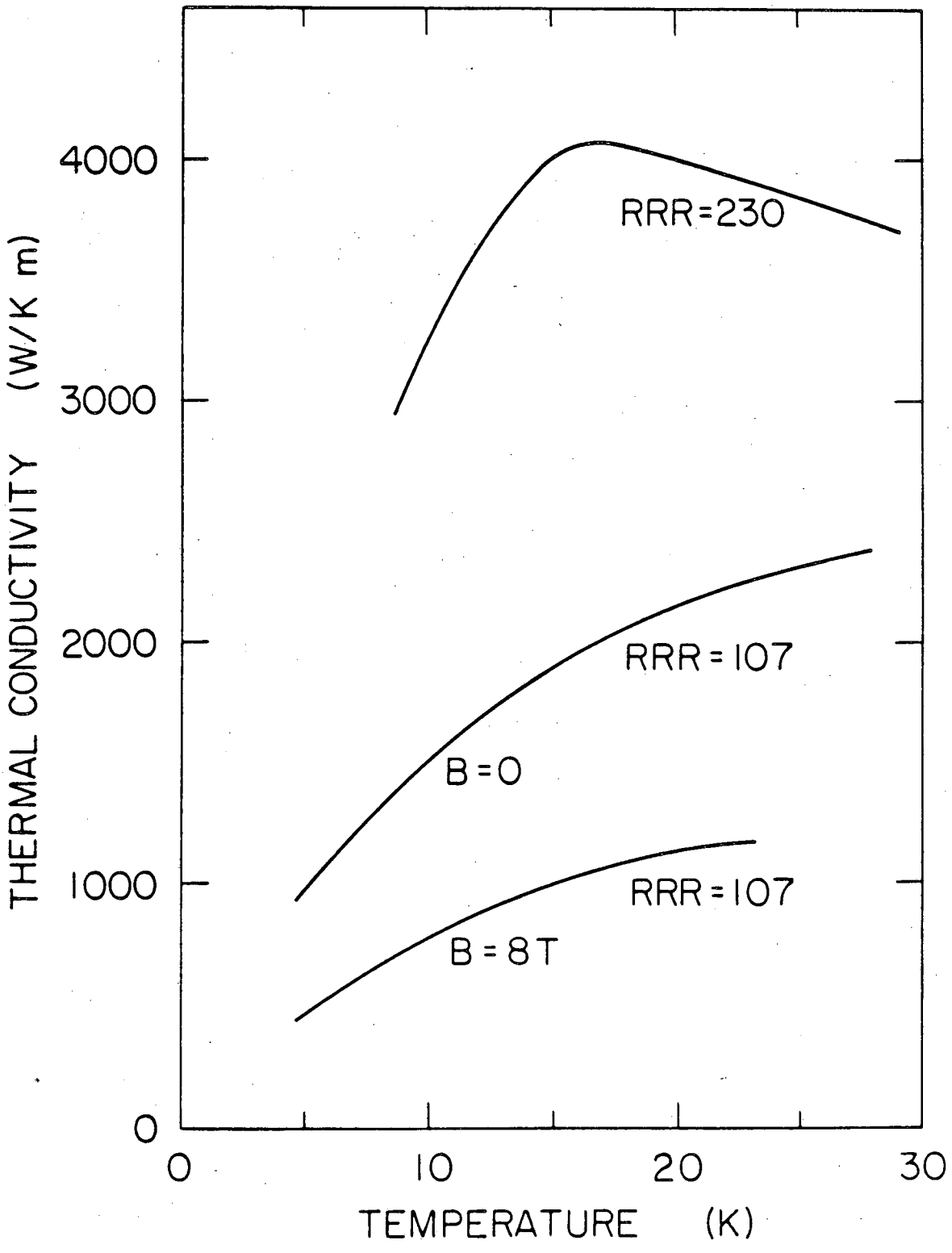

Fig. 54. The thermal conductivity of copper as a function of temperature.

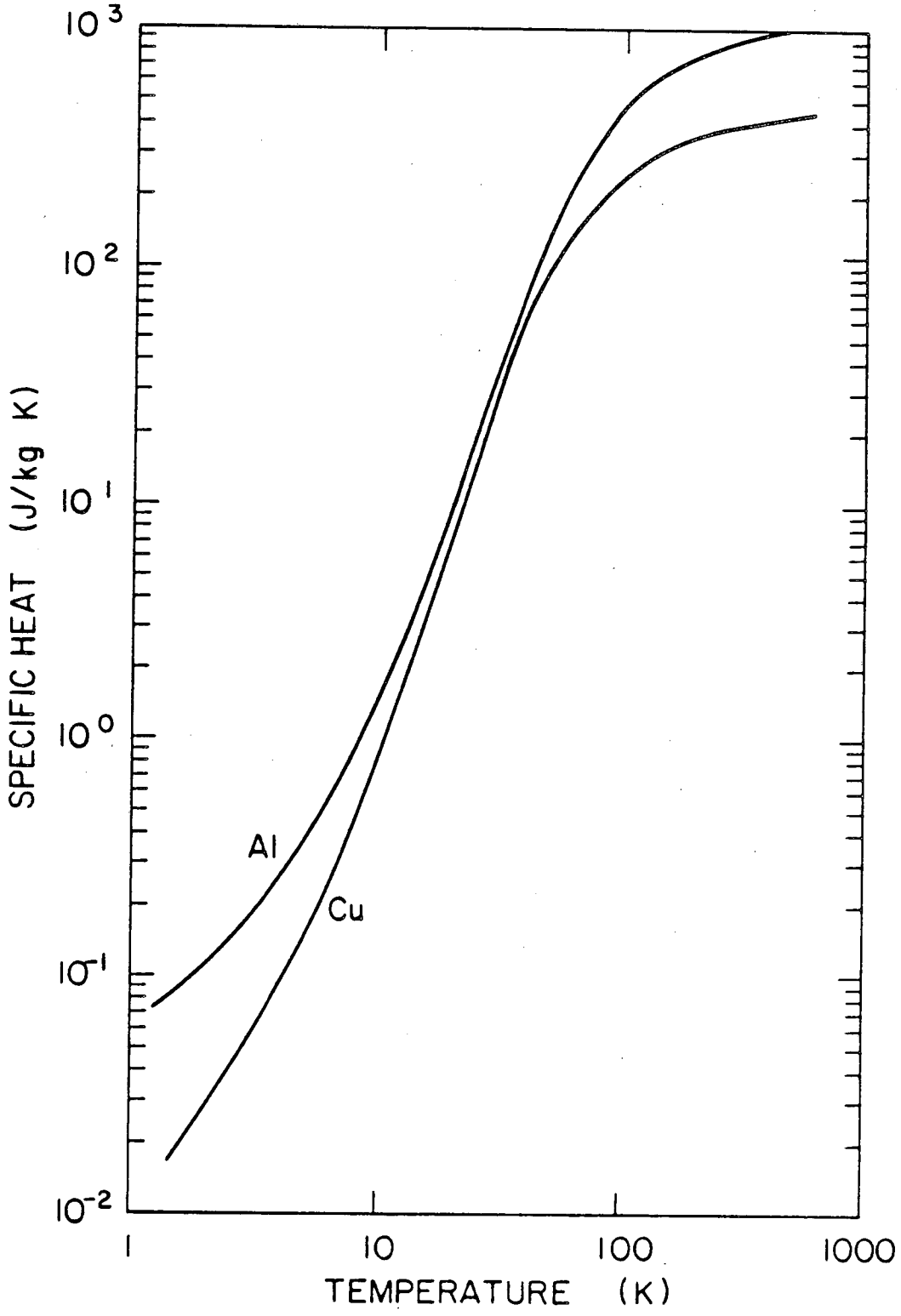

XBL 836-10140

Fig. 55. The specific heat of copper and aluminum as a function of temperature.

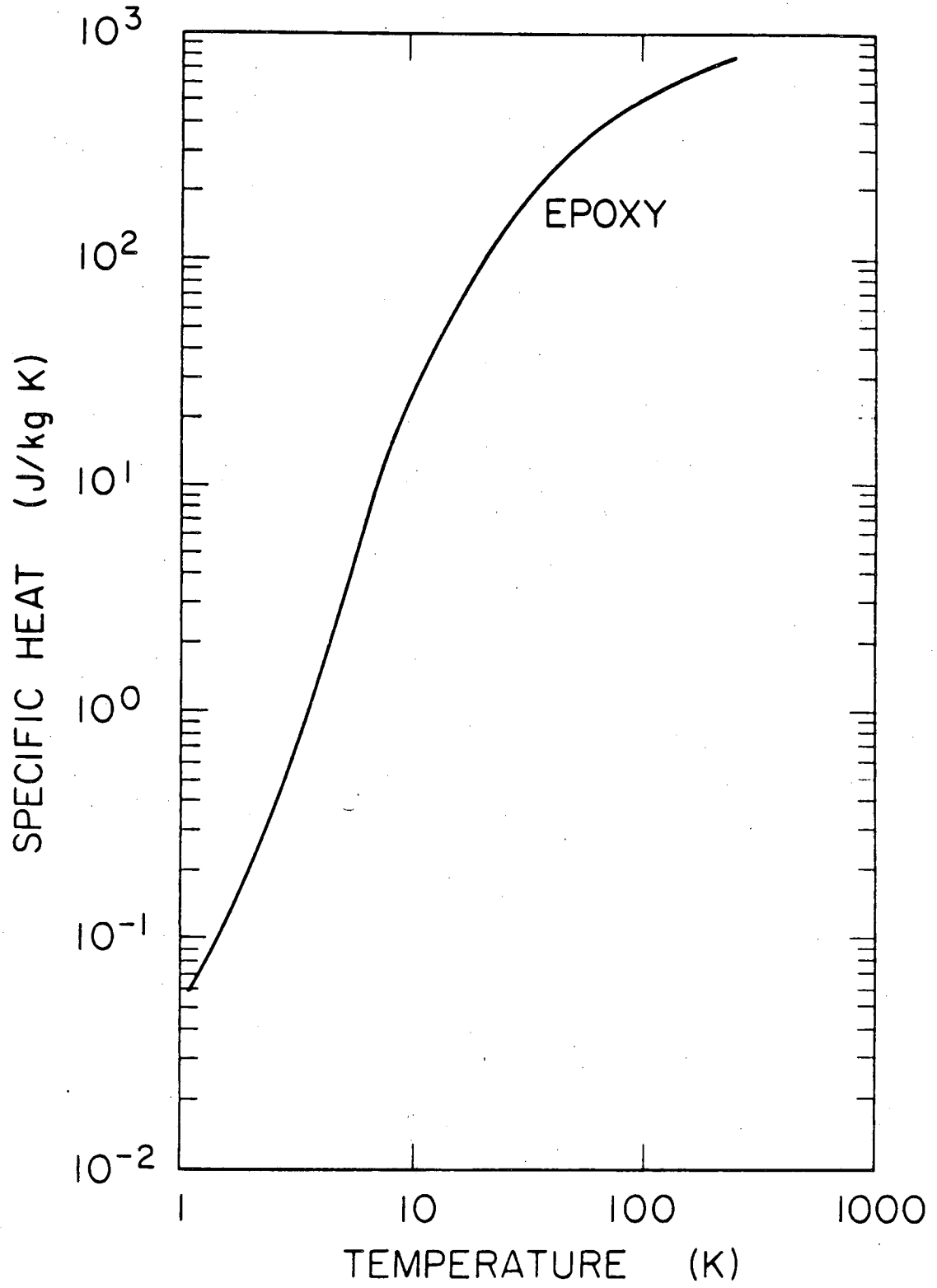

Fig. 56. The specific heat of epoxy as a function of temperature.

Though it is the specific heat of the conductors (normal and super) that affects stability, the specific heat of the insulating materials, including the enthalpy of the liquid helium, contribute to protection and safety by limiting the maximum temperature rise when a quench occurs.

V. Heat Transfer

We briefly described a heat transfer problem above when discussing thermal conductivity between two dissimilar materials. The most important heat transfer mechanism in a superconducting coil is from the conductor surface to the helium. The conductor and the bath are at two distinctly different temperatures during a disturbance and often during normal operation. For low temperature differences the conductivity of the helium itself, which is quite low, dominates. As the temperature increases bubble formation occurs and the heat transfer increases. At some point a maximum is reached and as the temperature increases the heat transfer drops as film boiling becomes the dominant mechanism. This "peak nucleate boiling" maximum, and the general shape of the boiling curve, see Fig. 57, vary some from conductor to conductor and depend on orientation and surface preparation.

Several characteristics of helium below the lambda point, 2.16K, make it a very effective fluid for cooling superconducting coils. They are discussed in Ref. 11 and include high transient heat transfer, a heat transfer characteristic that increases with temperature and high thermal conductivity in the fluid itself.

The maximum transient heat transfer observed in normal helium is about 10 W/cm for periods of a few milliseconds. Similar experiments

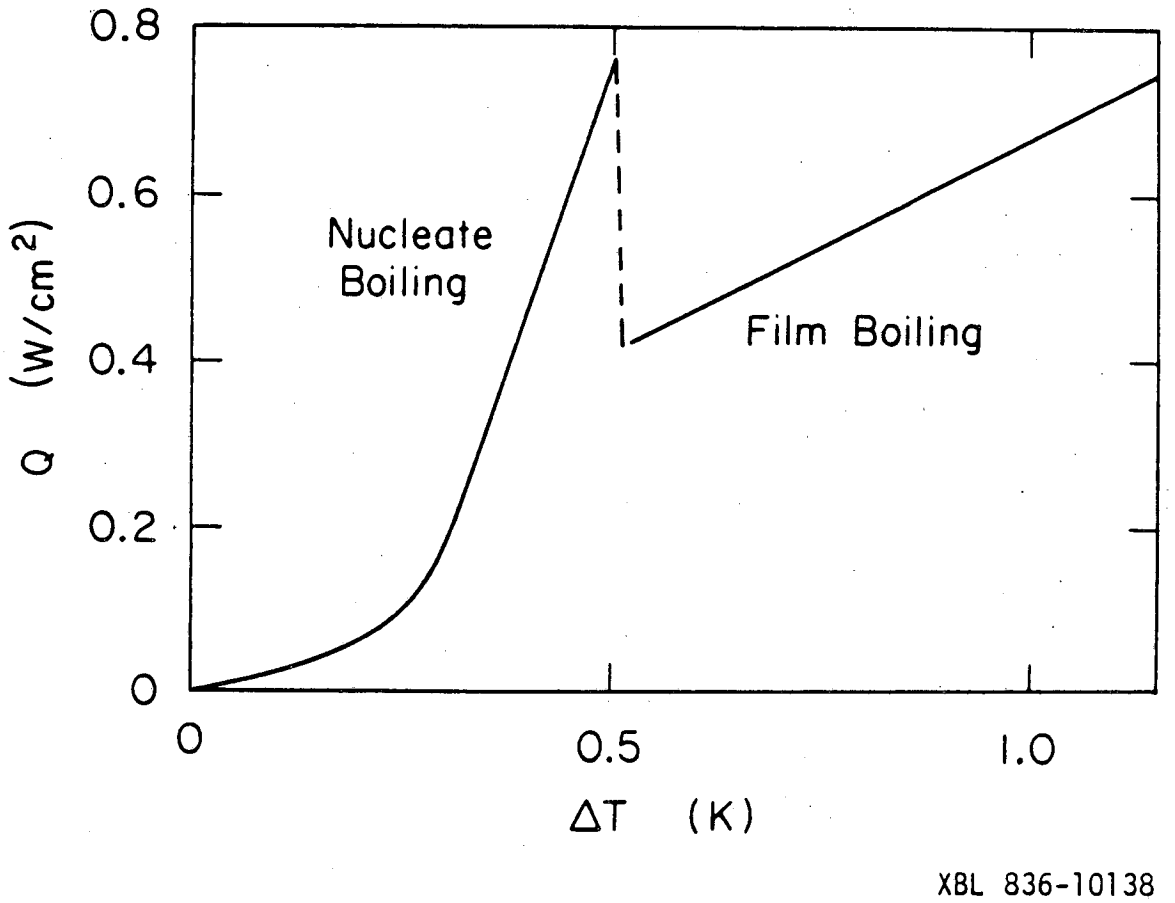

Fig. 57. The boiling curve for helium at 4.2K.

in superfluid helium show the transient heat transfer limit is greater than 40 W/cm^2.

The steady state heat transfer to superfluid helium is dominated by the Kapitza conductance at the solid-liquid interface. This mechanism yields a heat transfer characteristic of the form

$$q \propto \Delta T \cdot T^{2.8}$$

where the exponential 2.8 is empirical.

Heat removal over large distances is by a thermal conductivity in the fluid rather than by convection as in normal helium. This mechanism allows heat to be removed in many directions from a local hot spot, which is very important in high current density accelerator magnets which contain little helium and have restricted helium passages.

References

1. The proceedings of the Applied Superconductivity Conferences, Magnet Technology Conferences and Cryogenic Engineering Conferences contain many articles relevant to the technology of superconducting magnets.

2. D. C. Larbalestier, "Niobium Titanium Superconducting Materials," in Superconductor Material Science, eds. S. Foner and B. Schwartz, Plenum Press, N.Y., 1981, pp. 133-200.

3. M. N. Wilson, "Practical Superconducting Materials," ibid, pp. 63-133.

4. H. Brechner, Superconducting Magnet Systems, Springer-Verlag, Berlin, 1973.

5. Richard A. Beth, "Analytical Design of Superconducting Multipolar Magnets," Proceedings of the 1968 Summer Study on Superconducting Devices and Accelerators, Brookhaven National Laboratory, June 10-July 19, 1968. BNL 50155 (C-55).

6. Klaus Halbach, "Fields and First Order Perturbation Effects in Two-Dimensional Conductor Dominated Magnets," Nuclear Instruments and Methods, 78, 185 (1970).

7. I. I. Rabi, "A Method of Producing Uniform Magnetic Fields," Review of Scientific Instruments, 5, 78 (1934).

8. J. Rechen, Lawrence Berkeley Laboratory, unpublished.

9. R. B. Palmer, "Status Reports on Isabelle Magnets," Proceedings of the 1982 Applied Superconductivity Conference, Nov. 30-Dec. 3, 1982, Knoxville, Tennessee, to be published.

10. K. Leeb and H. H. Umstatter, "Magnets with Iron Yokes and Fields Above 20KG," CERN 66-7, Feb. 1966.

11. Stability of Superconductors, Proceedings of a workshop held at Saclay, France, Nov. 16-19, 1981, Commission A1/2, International Institute of Refrigeration, Paris, 1981.

TECHNICAL INFORMATION DEPARTMENT
LAWRENCE BERKELEY LABORATORY
UNIVERSITY OF CALIFORNIA
BERKELEY, CALIFORNIA 94720